Accepted Manuscript

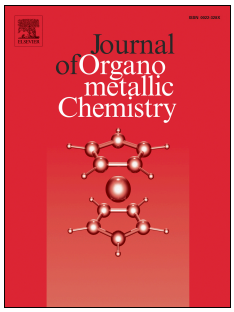

Synthesis, characterization, crystal structures, QSAR study and antibacterial activities of organotin bisphosphoramidates

Khodayar Gholivand, Ali Asghar EbrahimiValmoozi, Akram Gholami, Michal Dusek, Vaclav Eigner, Sara Abolghasemi

PII: S0022-328X(15)30159-5

DOI: 10.1016/j.jorganchem.2015.09.030

Reference: JOM 19245

To appear in: *Journal of Organometallic Chemistry*

Received Date: 9 May 2015

Revised Date: 22 September 2015

Accepted Date: 23 September 2015

Please cite this article as: K. Gholivand, A.A. EbrahimiValmoozi, A. Gholami, M. Dusek, V. Eigner, S. Abolghasemi, Synthesis, characterization, crystal structures, QSAR study and antibacterial activities of organotin bisphosphoramidates, *Journal of Organometallic Chemistry* (2015), doi: 10.1016/j.jorganchem.2015.09.030.

Graphical Abstract

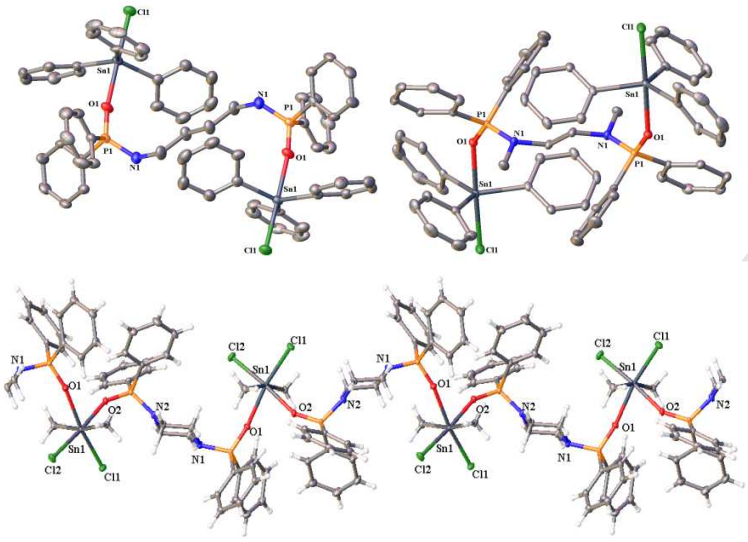

$$\text{Log } (1/\text{MIC}) = -14.093Q_{Sn} + 0.032L_{P\text{-}O} + 14.109PL_{Sn\text{-}O} - 33.098\omega + 0.001M\nu - 11.849$$

$n = 10$; $R^2 = 0.832$; $S_{reg} = 0.257$; $r = 0.103$; $F_{statistic} = 3.971$

Synthesis, characterization, crystal structures, QSAR study and antibacterial activities of organotin bisphosphoramidates

Khodayar Gholivand[a,*], Ali Asghar EbrahimiValmoozi[a], Akram Gholami[a], Michal Dusek[b], Vaclav Eigner[b], Sara Abolghasemi[a]

[a]*Department of Chemistry, Faculty of Sciences, TarbiatModares University, Tehran, Iran*

[b]*Institute of Physics of the ASCR, v.v.i., Na Slovance 2, 182 21 Praha 8, Czech Republic*

* Corresponding author's E-mail address: gholi_kh@modares.ac.ir

Tel.: +98 21 82883443; Fax: +98 218006544.

Abstract

Organotin complexes of bisphosphoramidates were prepared by the reaction of $SnR^1R^2R^3Cl$ (where R=alkyl/aryl/Cl) and $Ph_2P(O)XP(O)Ph_2$ ligands (where X=diamine). All the compounds were characterized by NMR and IR spectroscopy. X-Ray crystallography confirms that the bridging ligand produces binuclear complexes with $SnPh_3Cl$ acceptors in $\mathbf{C_{a3}}$ and $\mathbf{C_{a4}}$ and offers a polymeric structure toward $SnMe_2Cl_2$ in $\mathbf{C_{c5}}$. The synthesized compounds were screened for the antibacterial activity against *B. cereus* and *E. coli*. Based on the MIC test, the ligands are devoid of antibacterial activity. Notably, among the complexes, triphenyltin adducts exhibited **a** marked activity only against Gram-positive bacterium *B. Cereus* (IC_{50} = 0.78 μg/mL for $\mathbf{C_{a3}}$ and $\mathbf{C_{a5}}$). DFT–QSAR models revealed that the descriptor of the electrophilicity (ω) parameter is correlated with the inhibition activity on *B. cereus*. The correlation matrix of QSAR models and docking analysis confirmed that the electrophilicity parameter controls the influence of the net charge (Q_{Sn}) and polarizability of Sn atom of complexes on the inhibition of *B. cereus.*

Keywords: Bisphosphoramidate, Organotin compounds, Crystal structure, Antibacterial activity, QSAR

1. Introduction

Research on medicinal applications of metal complexes is an area of current interest and one of the most studied in biomedical and inorganic biochemistry. In this context, the potent therapeutic properties of tin complexes are well known [1-3]. The chemistry of organotins has received considerable attention during the last few decades owing to their industrial (catalysts in PVC and foam production), agricultural (fungicides and acaricides, wood preservatives) and medicinal applications (antibacterial and anticancer agents) [4-7]. Biological activity of organotin complexes is apparently correlated with the kind of the organic group and the donor ligand bound to tin [8], no method has been published so far to clarify the mechanism of the antibacterial potency of OTPA derivatives in the electronic and structural levels. To extend and evaluate this issue, new method is introduced by other authors in order to elucidate this mechanism. Quantitative structure–activity relationship (QSAR) equations enabled to create the correlation between the electronic and structural parameters of OTPA derivatives and the antibacterial activity [9-13]. From the above consideration, in connection with our current work on tin complexes of phosphoramidates [14-18] and to investigate the biological aspects of them, herein, we report synthesis and spectroscopic characterization (^{1}H, ^{13}C, ^{31}P, ^{119}Sn NMR and IR) of a series of organotin bisphosphoramidates prepared by the reaction of $SnR^1R^2R^3Cl$ (R = alkyl/aryl/Cl) and $Ph_2P(O)XP(O)Ph_2$ ligands where X = diamine (**Scheme 1**). The structure of ligand $\mathbf{L_4}$ and three complexes $\mathbf{C_{a3}}$, $\mathbf{C_{a4}}$ and $\mathbf{C_{c5}}$ were determined using X–ray crystallography. All the compounds were screened for the antibacterial activity against *B.*

cereus and *E. coli*. In order to understand the influence of electronic and structural properties for the titled compounds, an integrated molecular docking and QSAR models approaches were used to evaluate the binding interactions between the OTPA analogous and the *B. cereus*.

2. Experimental

2.1. Material and calculations

^{1}H, ^{31}P and ^{119}Sn NMR spectra were recorded on a Bruker Avance 300 spectrometer at 300.13, 121.50 and 111.86 MHz, respectively. ^{1}H chemical shifts were determined relative to internal TMS. ^{31}P and ^{119}Sn chemical shifts were measured relative to 85% H_3PO_4 and $SnMe_4$ as external standard respectively. Infrared (IR) spectra were recorded on a Shimadzu model IR-60 spectrometer using KBr pellets. Density functional calculations (DFT) at B3LYP level have been carried out using Gaussian 09 package [19]. The correlation analysis was performed by the Statistical Package for Social Scientists (SPSS), version 16.0 for Windows [20].

2.2. General procedure for the preparation of ligands

All the ligands were synthesized by the procedure reported in the literature [17]. A solution of diamine (1 mmol) and triethylamine (2 mmol, as HCl scavenger) in THF was added at 0 °C to a solution of diphenylposphinic chloride (2 mmol) in THF. After 4 h stirring, the solvent was removed in vacuum and the resulting was washed with distilled

water. Compound **L_4** was recrystallized from a mixture of THF and H_2O at room temperature to obtain crystals suitable for X-ray analysis. Physical and spectroscopic data of new ligands (**L_1**-**L_4** and **L_6**) are presented below. Characterization of **L_5** and **L_7** were reported in our previous work [17].

$Ph_2P(O)NH–(CH_2)_2–HNP(O)Ph_2$ (***L_1***)

Mp: 228–230 °C. ^{1}H NMR (d6–DMSO, ppm); δ= 2.88 (m, 4H, CH_2), 5.51 (m, 2H, NH), 7.43–7.47 (m, 8H, Ph), 7.49–7.52 (m, 4H, Ph), 7.73–7.77 (m, 8H, Ph). ^{13}C NMR (d6–DMSO, ppm); δ= 42.0 (d, $^2J_{PC}$ = 6.1 Hz, CH_2), 128.3 (d, $^3J_{PC}$ = 12.1 Hz, *m*–Ph), 131.4 (s, *p*–Ph), 131.6 (d, $^2J_{PC}$ = 9.4 Hz, *o*–Ph), 133.6 (d, $^1J_{PC}$ = 126.5 Hz, *ipso*–Ph). ^{31}P{^{1}H} NMR (d6–DMSO, ppm); δ= 21.9 (m). IR (KBr, cm^{-1}): $\tilde{\upsilon}$ = 3199 (N–H), 2928 (s), 1438 (s), 1186 (s, P=O), 1111 (s), 722 (m).

$Ph_2P(O)NH–(CH_2)_3–HNP(O)Ph_2$ (***L_2***)

Mp: 222–225 °C. ^{1}H NMR (d6–DMSO, ppm); δ= 1.60 (q, 2H, β-CH_2), 2.84 (td, 4H, α-CH_2), 5.37 (m, 2H, NH), 7.44–7.47 (m, 8H, Ph), 7.49–7.52 (m, 4H, Ph), 7.72–7.76 (m, 8H, Ph). ^{13}C NMR (d6–DMSO, ppm); δ= 33.1 (m, β-CH_2), 37.3 (s, α-CH_2), 128.4 (d, $^3J_{PC}$ = 12.0 Hz, *m*–Ph), 131.4 (s, *p*–Ph), 131.6 (d, $^2J_{PC}$ = 9.2 Hz, *o*–Ph), 133.9 (d, $^1J_{PC}$ = 126.1 Hz,, *ipso*–Ph). ^{31}P{^{1}H} NMR (d6–DMSO, ppm); δ= 21.8 (m) ppm. IR (KBr): $\tilde{\upsilon}$ = 3178 (N–H), 2921 (s), 1437 (s), 1180 (s, P=O), 1120 (s), 725 (m).

$Ph_2P(O)NH–(CH_2)_4–HNP(O)Ph_2$ (***L_3***)

Mp: 186–188 °C. ^{1}H NMR (d6–DMSO, ppm); δ= 1.61 (m, 4H, β-CH_2), 2.93 (m, 4H, α-CH_2), 5.18 (m, 2H, NH), 7.39–7.44 (m, 8H, Ph), 7.45–7.48 (m, 4H, Ph), 7.82–7.89 (m,

8H, Ph). ^{13}C NMR (d6–DMSO, ppm); δ= 29.1 (m, β-CH_2), 38.0 (m, α-CH_2), 128.9 (d, $^3J_{PC}$ = 12.0 Hz, *m*–Ph), 131.9 (s, *p*–Ph), 132.1 (d, $^2J_{PC}$ = 9.2 Hz, *o*–Ph), 134.5 (d, $^1J_{PC}$ = 126.0 Hz, *ipso*–Ph). ^{31}P{^{1}H} NMR (d6–DMSO, ppm); δ= 23.8 (m). IR (KBr, cm^{-1}): $\tilde{\upsilon}$ = 3247 (m, N–H), 2939 (s), 1431 (s), 1188(s, P=O), 1115 (s), 722 (m).

*$Ph_2P(O)NMe–(CH_2)_2$-NMeP(O)Ph_2 (**L_4**)*

Mp: 199–201 °C. ^{1}H NMR (d6–DMSO, ppm); δ= 2.38 (d, $^3J_{P–H}$ = 10.8 Hz, 6H, CH_3), 3.07–3.09 (m, 4H, CH_2), 7.39–7.44 (m, 8H, Ph), 7.46–7.49 (m, 4H, Ph), 7.76–7.80 (m, 8H, Ph). ^{13}C NMR (d6–DMSO, ppm); δ= 34.3 (d, $^2J_{PC}$ = 2.6 Hz, CH_3), 47.4 (m, CH_2), 128.6 (d, $^3J_{PC}$ = 12.5 Hz, *m*–Ph), 131.9 (s, *p*–Ph), 132.2 (d, $^2J_{PC}$ = 9.1 Hz, *o*–Ph), 131.4 (d, $^1J_{PC}$ = 128.5 Hz,, *ipso*–Ph). ^{31}P{^{1}H} NMR (d6–DMSO, ppm); δ= 31.6 (m). IR (KBr, cm^{-1}): $\tilde{\upsilon}$ = 2930 (s), 1441 (s), 1161 (s, P=O), 1112 (s), 984 (s), 731 (m).

*1,4-[$Ph_2P(O)O$-C_6H_4-$OP(O)Ph_2$] (**L_6**)*

Mp: 206-208 °C. ^{1}H NMR (DMSO-d_6, ppm): δ = 7.16 (s, 4H, Ph), 7.51-7.60 (m, 12H, 4Ph), 7.71-7.84 (m, 8H, 4Ph). ^{31}P NMR (DMSO-d_6, ppm): δ = 29. 8. [^{1}H NMR ($CDCl_3$, ppm): δ = 7.06 (s, 4H, Ph), 7.40-7.56 (m, 12H, 4Ph), 7.79-7.86 (m, 8H, 4Ph). ^{31}P NMR ($CDCl_3$, ppm): δ = 28.4.] Selected IR data (KBr, cm^{-1}): $\tilde{\upsilon}$ = 1235 (s), 1180 (s, P=O), 914 (s).

2.3. General procedure for the preparation of complexes

The complexes were prepared by using the similar procedure: Methanol-chloroform solutions of 2 eq. organotin chloride ($SnMe_2Cl_2$, $SnPh_3Cl$, $SnPh_2Cl_2$ or $SnPhCl_3$) with 1 eq. the bisphosphoramide ligand were mixed. Suitable crystals of $\mathbf{C_{a3}}$, $\mathbf{C_{a4}}$ and $\mathbf{C_{c5}}$ for X–ray diffraction were obtained from slow evaporation of the solution at room temperature. Physical and spectroscopic data of the complexes are given below: Characterization of $\mathbf{L_5}$ and $\mathbf{L_7}$ were reported in our previous work [17].

μ-[$Ph_2P(O)NH–(CH_2)_2–HNP(O)Ph_2$][$SnPh_3Cl$]$_2$ ***(C_{a1})***

M.p. 138-140 °C. ^{1}H NMR (CD_3OD, ppm): δ= 2.99–3.03 (m, 4H, CH_2), 7.43–7.55 (m, 30H, Ph-P + *m*, *p*-Ph-Sn), 7.76-7.84 (m, 20H, $^3J(^{119/117}Sn, ^1H)$ = 58.6Hz, Ph-P + *o*-Ph-Sn). ^{13}C NMR (CD_3OD, ppm): δ= 37.1 (d, $^3J_{PC}$ = 19.2 Hz, CH_2), 128.4 (s, $^3J(^{119/117}Sn, ^{13}C)$ = 73.0 Hz, *m*-Ph-Sn), 128.6 (s, *m*–Ph-P), 129.2 (s, *p*–Ph-Sn), 131.6 (s, *o*–Ph-P), 131.8 (s, *p*–Ph-P), 132.0 (s, *ipso*–Ph-P), 136.0 (s, $^2J(^{117/119}Sn, ^{13}C)$ = 47.0 Hz, *o*-Ph-Sn). ^{31}PNMR (CD_3OD, ppm): δ = 24.6 (m). ^{119}Sn NMR (CD_3OD, ppm): δ = -181.0 ppm. IR (KBr, cm^{-1}): $\tilde{\upsilon}$ = 3175 (m, N–H), 2928 (m), 1434 (w), 1306 (w), 1177 (s, P=O), 1111 (s), 868 (w), 727 (w), 694.9 (w), 554 (w), 447 (w).

[*$Ph_2P(O)NH–(CH_2)_2–HNP(O)Ph_2$.$SnPh_2Cl_2$*]$_n$ ***(C_{b1})***

M.p. 176-178 °C. ^{1}H NMR (CD_3OD, ppm): δ= 3.18 (m, 4H, CH_2), 7.46–7.75 (m, 18H, Ph-P + Ph-Sn), 7.90-8.03 (m, 12H, Ph-P + Ph-Sn). ^{13}C NMR (CD_3OD, ppm): δ= 41.0 (m, CH_2), 128.4 (s, $^3J(^{119/117}Sn, ^{13}C)$ = 100 Hz, *m*-Ph-Sn), 128.6 (s, *m*-Ph-P), 128.8 (s, *p*-Ph-Sn), 131.2-131.6 (m, Ph-P), 135.9 (s, *o*-Ph-Sn). ^{31}P NMR (CD_3OD, ppm): δ = 24.9 (m).

^{119}Sn NMR (CD_3OD, ppm): δ = low solubility. IR (KBr, cm^{-1}): $\tilde{\upsilon}$ = 3391 (m, N–H), 3056 (m), 1432 (w), 1131 (s, P=O), 866 (w), 735 (w), 693.8 (w), 558 (w), 457 (w).

*$[Ph_2P(O)NH–(CH_2)_2–HNP(O)Ph_2.SnMe_2Cl_2]_n$ (**C_{c1}**)*

M.p. 174-176 °C. Anal. Calc. for $C_{28}H_{32}Cl_2N_2O_2P_2Sn$: C, 49.45; H, 4.74; N, 4.12; found: C, 44.72; H, 4.79; N, 3.69%. ^{1}H NMR (CD_3OD, ppm): δ = 1.08 (s, 6H, $^2J(^{119/117}Sn, ^1H)$ = 91.5 Hz, Me-Sn), 3.02–3.22 (m, 4H, CH_2), 7.47–7.56 (m, 12H, Ph), 7.76–7.86 (m, 8H, Ph). ^{13}C NMR (CD_3OD, ppm): δ = 38.2 (s, Sn–Me), 42.2 (m, CH_2), 128.4-128.8 (m, Ph), 131.2-132.6 (m, Ph). ^{31}P NMR (CD_3OD, ppm): δ = 24.6 (m). ^{119}Sn NMR (CD_3OD, ppm): δ= -245.5 ppm. IR (KBr, cm^{-1}): $\tilde{\upsilon}$ = 3247 (m, N–H), 2925 (m), 1434 (w), 1146 (s, P=O), 945 (w), 750 (w), 693 (w), 559 (w), 448 (w).

*μ-$[Ph_2P(O)NH–(CH_2)_3–HNP(O)Ph_2][SnPh_3Cl]_2$ (**C_{a2}**)*

M.p. 105-107 °C.^{1}H NMR (CD_3OD, ppm): δ= 1.74 (t, $^2J_{HH}$ = 6.7 Hz, 2H, β-CH_2), 2.95–2.98 (m, 4H, α-CH_2), 7.43–7.59 (m, 30H, Ph-P + Ph-Sn), 7.75–7.98 (m, 20H, Ph-P + Ph-Sn). ^{13}C NMR (CD_3OD, ppm): δ= 29.3 (m, β-CH_2), 37.2 (m, α-CH_2), 128.3-129.1 (m, *m*-Ph-P + *m*, *p*-Ph-Sn), 131.2-132.6 (m, Ph-P), 136.0 (s, *o*-Ph-Sn). ^{31}P NMR (CD_3OD, ppm): δ = 24.4 (m). ^{119}Sn NMR (CD_3OD, ppm): δ = -181.2 ppm. IR (KBr, cm^{-1}): $\tilde{\upsilon}$ = 3181 (m, N–H), 3055.1 (s), 2929 (m), 1431 (w), 1304 (w), 1156 (s, P=O), 1117 (s), 863 (w), 731 (w), 694 (w), 554 (w), 449 (w).

*$[Ph_2P(O)NH–(CH_2)_3–HNP(O)Ph_2.SnPh_2Cl_2]_n$ (**C_{b2}**)*

M.p. 161-163 °C. Anal. Calc. for $C_{39}H_{38}Cl_2N_2O_2P_2Sn$: C, 57.24; H, 4.68; N, 3.42; found: C, 58.74; H, 5.18; N, 3.81%. ^{1}H NMR (CD_3OD, ppm): δ= 1.78 (t, $^2J_{HH}$ = 7.5 Hz, 2H, β-CH_2), 2.94–3.08 (m, 4H, α-CH_2), 7.52–7.56 (m, 18H, Ph-P + Ph-Sn), 7.79–7.85 (m, 12H, Ph-P + Ph-Sn). ^{13}C NMR (CD_3OD, ppm): δ= 33.3 (m, β-CH_2), 37.6 (m, α-CH_2), 128.36 (s, ^3J($^{119/117}$Sn, ^{13}C) = 85.9 Hz, *m*-Ph-Sn), 128.6 (s, *m*-Ph-P), 129.3 (s, *p*-Ph-Sn), 131.6 (s, *p*-Ph-P), 131.8 (s, *o*-Ph-P), 132.0 (s, *ipso*-Ph-P), 136.0 (s, ^2J($^{119/117}$Sn, ^{13}C) = 48.0 Hz, *o*-Ph-Sn). ^{31}P NMR (CD_3OD, ppm): δ = 25.6 (m). ^{119}Sn NMR (CD_3OD, ppm): δ = -452.5 ppm. IR (KBr, cm^{-1}): $\tilde{\upsilon}$ = 3386 (m, N–H), 3056 (m), 1434 (w), 1126 (s, P=O), 993 (w), 730 (w), 694 (w), 556 (w), 451 (w).

[$Ph_2P(O)NH–(CH_2)_3–HNP(O)Ph_2.SnMe_2Cl_2]_n$ (***C_{c2}***)

M.p. 107 °C. ^{1}H NMR (CD_3OD, ppm): δ = 1.08 (s, 6H, ^2J($^{119/117}$Sn, ^{1}H) = 95.0 Hz, Me-Sn), 1.76 (t, $^2J_{HH}$ = 6.7 Hz, 2H, β-CH_2), 2.95–3.08 (m, 4H, α-CH_2), 7.48–7.59 (m, 12H, Ph), 7.76–7.87 (m, 8H, Ph). ^{13}C NMR (CD_3OD, ppm): *low solubility*. ^{31}P NMR (CD_3OD, ppm): δ = 24.5 (m). ^{119}Sn NMR (CD_3OD, ppm): δ = -120.4 ppm. IR (KBr, cm^{-1}): $\tilde{\upsilon}$ = 3278 (N–H), 2924 (m), 1443 (w), 1157 (s, P=O), 802 (w), 735 (w), 687 (w), 555 (w), 449 (w).

μ-[$Ph_2P(O)NH–(CH_2)_4–HNP(O)Ph_2$][$SnPh_3Cl$]$_2$ (***C_{a3}***)

M.p. 117-120 °C. Anal. Calc. for $C_{64}H_{60}Cl_2N_2O_2P_2Sn_2$: C, 61.03; H, 4.80; N, 2.22; found: C, 61.07; H, 4.98; N, 2.38%. ^{1}H NMR (CD_3OD, ppm): δ= 1.56 (m, 4H, β-CH_2), 2.83 (m, 4H, α-CH_2), 7.44–7.58 (m, 30H, Ph-P + *m*, *p*-Ph-Sn), 7.72–7.98 (m, 20H, ^3J($^{119/117}$Sn,^{1}H) = 59.0 Hz, Ph-P + *o*–Ph-Sn). ^{13}C NMR (CD_3OD, ppm): δ= 28.8 (d, $^3J_{PC}$ = 6.4 Hz, β-

CH_2), 40.0 (m, α-CH_2), 128.3 (s, $^{3}J(^{119/117}Sn, ^{13}C)$ = 71.0 Hz, *m*-Ph-Sn), 128.5 (s, *m*–Ph-P), 129.2 (s, *p*–Ph-Sn), 131.7 (s, *o*–Ph-P), 131.8 (s, *p*–Ph-p), 132.0 (s, *ipso*–Ph-P), 136.0 (s, $^{3}J(^{117/119}Sn–^{13}C)$ = 47.5 Hz, *o*-Ph-Sn). ^{31}P NMR (CD_3OD, ppm): δ = 24.3 (m). ^{119}Sn NMR (CD_3OD, ppm): δ = -180.5 ppm. IR (KBr, cm^{-1}): $\tilde{\upsilon}$ = 3362 (m, N–H), 3055 (s), 2941 (m), 1428 (w), 1307 (w), 1157 (s, P=O), 1110 (s), 837.3 (w), 731 (w), 695 (w), 561 (w), 449 (w).

*$[Ph_2P(O)NH–(CH_2)_4–HNP(O)Ph_2.SnPh_2Cl_2]_n$ (**C_{b3}**)*

^{1}H NMR (CD_3OD, ppm): δ= 1.55–1.70 (m, 4H, β-CH_2), 2.99–3.10 (m, 4H, α-CH_2), 7.58–7.66 (m, 18H, Ph-P + Ph-Sn), 7.88–7.97 (m, 12H, Ph-P + Ph-Sn). ^{13}C NMR (CD_3OD, ppm): δ= 28.6 (d, $^{4}J_{PC}$ = 4.7 Hz, β-CH_2), 42.8 (m, α-CH_2), 127.2 (s, $^{3}J(^{117/119}Sn, ^{13}C)$ = 123.2 Hz, *m*-Ph-Sn), 127.7 (s, *p*-Ph-Sn), 128.4 (d, $^{3}J_{PC}$ = 11.9 Hz, 8C, *m*–Ph-P), 131.4 (s, *p*–Ph-P), 131.7 (d, $^{2}J_{PC}$ = 9.2 Hz, *o*–Ph-P), 133.1 (s, *ipso*–Ph-P), 134.7 (s, $^{3}J(^{117/119}Sn, ^{13}C)$ = 71.9 Hz, *o*-Ph-Sn), 155.5 (s, *ipso*-Ph-Sn). ^{31}P NMR (CD_3OD, ppm): δ 24.5 (m). ^{119}Sn NMR (CD_3OD, ppm): δ = -471.5 ppm. IR (KBr, cm^{-1}): $\tilde{\upsilon}$ = 3343 (m, N–H), 3053 (m), 2942 (s), 1433 (w), 1148 (s, P=O), 936 (w), 732 (w), 695 (w), 553 (w), 455 (w).

*$[Ph_2P(O)NH–(CH_2)_4–HNP(O)Ph_2.SnMe_2Cl_2]_n$ (**C_{c3}**)*

^{1}H NMR (d6–DMSO, ppm): δ = 1.03 (6H, $^{2}J(^{119/117}Sn, ^{1}H)$ = 111.8 Hz, Me-Sn), 1.47 (m, 4H, β-CH_2), 2.66–2.69 (m, 4H, α-CH_2), 5.24–5.27 (m, 2H, NH), 7.42–7.52 (m, 12H, Ph), 7.72–7.78 (m, 8H, Ph). ^{13}C NMR (CD_3OD, ppm): δ = 38.2 (s, Sn–Me), 40.9 (m, β-CH_2), 42.2 (m, α-CH_2), 128.4-128.8 (m, Ph), 131.2-132.6 (m, Ph). ^{31}P NMR (CD_3OD, ppm): δ

= 26.9 (m). ^{119}Sn NMR (d6–DMSO, ppm): δ = low solubility. IR (KBr, cm^{-1}): $\tilde{\upsilon}$ = 2930 (m), 1434 (w), 1144 (s, P=O), 796 (w), 731 (s), 694 (w), 559 (w), 448 (w).

μ-[$Ph_2P(O)NMe–(CH_2)_2–NMeP(O)Ph_2$][$SnPh_3Cl$]$_2$ (***C$_{a4}$***)

M.p. 217-2219 °C.^{1}H NMR (CD_3OD, ppm): δ= 2.53–2.57 (m, 6H, Me), 3.21–3.25 (m, 4H, CH_2), 7.54–7.75 (m, 30H, Ph-P + Ph-Sn), 7.89–7.96 (m, 20H, Ph-P + Ph-Sn). ^{13}C NMR (CD_3OD, ppm): δ= 33.7 (s, Me), 46.5 (s, CH_2), 128.3 (s, Ph-Sn), 128.9 (s, Ph-Sn), 128.7 (d, $^3J_{PC}$ = 12.1 Hz, *m*–Ph-P), 131.1 (s, *p*–Ph-P), 131.9 (d, $^2J_{PC}$ = 9.3 Hz, *o*–Ph-P), 132.9 (s, *ipso*–Ph-P), 136.0 (s, ^3J($^{117/119}$Sn, ^{13}C) = 67.8 Hz, *m*-Ph-Sn) 162.0 (s, *ipso*-Ph-Sn). ^{31}PNMR (CD_3OD, ppm): δ = 31.5 (m). ^{119}Sn NMR (CD_3OD, ppm): δ = -153.3 ppm. IR (KBr, cm^{-1}): $\tilde{\upsilon}$ = 2931 (m), 1435 (w), 1309 (w), 1138 (s, P=O), 991 (s), 731 (w), 696 (w), 557 (w), 454 (w).

[$Ph_2P(O)NMe–(CH_2)_2–NMeP(O)Ph_2$.$SnPh_2Cl_2$]$_n$ (***C$_{b4}$***)

Anal. Calc. for $C_{40}H_{40}Cl_2N_2O_2P_2Sn$: C, 57.72; H, 4.84; N, 3.37; found: C, 56.88; H, 5.05; N, 3.52%. ^{1}H NMR (CD_3OD, ppm): δ= 2.53–2.57 (m, 6H, Me), 2.91–3.23 (m, 4H, CH_2), 7.59–7.75 (m, 20H, Ph-P + Ph-Sn), 7.88–7.99 (m, 10H, Ph-P + Ph-Sn). ^{13}C NMR (CD_3OD, ppm): δ= 128.6-137.2 (m, Ph-P + Ph-Sn).^{31}PNMR (CD_3OD, ppm): δ = 31.2 (m). ^{119}Sn NMR (CD_3OD, ppm): δ = -156.0 ppm. IR (KBr, cm^{-1}): $\tilde{\upsilon}$ = 3055 (m), 1438 (w), 1144 (s, P=O), 994 (w), 734 (w), 696 (w), 561 (w), 463 (w).

μ-[$Ph_2P(O)N(C_4H_8)NP(O)Ph_2$][$SnPh_3Cl$]$_2$ (***C$_{a5}$***) *[17]*

^{1}H NMR (CD_3OD, ppm): δ = 3.10 (m, 8 H, C_4H_8), 7.50–7.57 (m, 12H, Ph-P), 7.80–7.91 (m, 8H, Ph-P), 7.44–7.51 (m, 18H, *m*, *p*–Ph-Sn), 7.67–7.70 (m, 12H, *o*-Ph-Sn). ^{13}C NMR (CD_3OD, ppm): *δ*= 44.52–44.62 (m, C_4H_8), 128.4 (s, $^{3}J(^{119/117}Sn, ^{13}C)$ = 59.5 Hz, *m*-Ph-Sn), 128.7 (s, *p*-Ph-Sn), 128.9 (d, $^{3}J_{PC}$ = 8.4 Hz, *m*-Ph-P), 130.6 (s, *p*-Ph-P), 132.0 (d, $^{3}J_{PC}$ = 7.8 Hz, *o*-Ph-P), 132.2 (s, *ipso*-Ph-P), 136.0 (s, $^{2}J(^{119/117}Sn, ^{13}C)$ = 39.8 Hz, *o*-Ph-Sn). ^{31}P NMR (CD_3OD, ppm): δ = 31.8. ^{119}Sn NMR (CD_3OD, ppm): δ = -180.7 ppm. IR (KBr, cm^{-1}): $\tilde{\upsilon}$ = 2906 (m), 1431 (w), 1150 (s, P=O), 1120 (s), 958 (w), 727 (w), 696 (w), 544 (w), 450 (w).

$[Ph_2P(O)N(C_4H_8)NP(O)Ph_2.SnPh_2Cl_2]_n$ ***(C_{b5})***

^{1}H NMR (CD_3OD, ppm): δ = 2.93 (m, 8H, C_4H_8), 7.24–7.36 (m, 6H, Ph), 7.46-7.57 (m, 10H, Ph), 7.75–7.81 (m, 8H, Ph), 7.89–7.91 (m, 6H, Ph). ^{13}C NMR (CD_3OD, ppm): *low solubility*. ^{31}P NMR (CD_3OD, ppm): δ = 32.1. ^{119}Sn NMR (CD_3OD, ppm): δ = -74.6. IR (KBr, cm^{-1}): $\tilde{\upsilon}$ = 3056 (m), 1437 (w), 1139 (s, P=O), 10718 (s), 971 (w), 724 (w), 697 (w), 552 (w), 457 (w).

$[Ph_2P(O)N(C_4H_8)NP(O)Ph_2.SnMe_2Cl_2]_n$ ***(C_{c5})***

^{1}H NMR (CD_3OD, ppm): *δ* = 1.03 (6H, $^{2}J(^{119/117}Sn, ^{1}H)$ = 111.3 Hz, Me-Sn), 2.93–2.95 (m, 8H, C_4H_8), 7.46–7.56 (m, 12H, Ph), 7.74–7.81 (m, 8H, Ph). ^{13}C NMR (CD_3OD, ppm): *δ*= 41.8 (s, Me-Sn), 44.9 (m, C_4H_8), 128.5-129.2 (m, Ph), 131.2-132.9 (m, Ph). ^{31}P NMR (CD_3OD, ppm): δ = 31.5. ^{119}Sn NMR (CD_3OD, ppm): δ = *low solubility*. IR (KBr, cm^{-1}): $\tilde{\upsilon}$ = 3061, 2920, 1438 (w), 1154 (s, P=O), 1119 (m), 965 (w), 935, 784, 722 (w), 582 (w), 545 (w).

*μ-[1,4-$Ph_2P(O)O$-C_6H_4-$OP(O)Ph_2$][$SnPh_3Cl$]$_2$ (**C_{a6}**) [17]*

Mp: 171-173 °C. ^{1}H NMR ($CDCl_3$, ppm): δ = 7.04 (s, 4H, C_6H_4), 7.41–7.57 (m, 30H, Ph-P + Ph-Sn), 7.66–7.70 (m, 12H, $^3J(^{119/117}Sn,^1H)$ = 60 Hz, *o*-Ph_3Sn), 7.79–7.86 (m, 8H, Ph-P). ^{31}P NMR ($CDCl_3$, ppm): δ = 28.5. ^{119}Sn NMR ($CDCl_3$, ppm): δ = -49.7. IR (KBr, cm^{-1}): $\tilde{\upsilon}$ = 1210, 1173 (s, P=O), 918 (s).

*μ-[1,4-$Ph_2P(O)O$-C_6H_4-$OP(O)Ph_2$][$SnPh_2Cl_2$]$_2$ (**C_{b6}**)*

Mp: 191-193 °C. ^{1}H NMR ($CDCl_3$, ppm): δ = 6.95 (s, 4H, C_6H_4), 7.40–7.57 (m, 24H, Ph-P + Ph-Sn), 7.70–7.74 (m, 8H, $^3J(^{119/117}Sn,^1H)$ = 60 Hz, *o*–Ph-Sn), 7.76–7.81 (m, 8H, Ph-P). ^{31}P NMR ($CDCl_3$, ppm): δ = 28.6. ^{119}Sn NMR ($CDCl_3$, ppm): δ = -66.0. IR (KBr, cm^{-1}): $\tilde{\upsilon}$ = 1163 (P=O), 936 (s).

*μ-[1,4-$Ph_2P(O)O$-C_6H_4-$OP(O)Ph_2$][$SnPhCl_3$]$_2$ (**C_{d6}**)*

Mp: 1196-198 °C ^{1}H NMR ($CDCl_3$, ppm): δ = 6.91 (s, 4H, C_6H_4), 7.38–7.50 (m, 14H, Ph-P + Ph-Sn), 7.59–7.68 (m, 8H, Ph-Sn), 7.76–7.80 (m, 8H, Ph-P). ^{31}P NMR ($CDCl_3$, ppm): δ = 30.2. ^{119}Sn NMR ($CDCl_3$, ppm): δ = -54.0. IR (KBr, cm^{-1}): $\tilde{\upsilon}$ = 1166 (P=O), 933 (s).

*μ-[1,3-($Ph_2P(O)NHCH_2$)$_2C_6H_4$][$SnPh_3Cl$]$_2$ (**C_{a7}**)*

Mp: 171-173 °C. ^{1}H NMR ($CDCl_3$, ppm): δ = 3.11 (ps-q, 2H, $^3J_{PH}$ = 5.8 Hz, N–H), 3.96 (ps-t, 4H, $^3J_{PH}$ = 7.6 Hz, CH_2), 7.19–7.27 (m, 4H, C_6H_4), 7.41–7.49 (m, 30H, Ph-P + Ph-Sn), 7.75–7.87 (m, 20H, $^3J(^{119/117}Sn,^1H)$ = 63 Hz, Ph-P + *o*–Ph-Sn). ^{31}P NMR (CDCl3,

ppm): δ =24.5. ^{119}Sn NMR ($CDCl_3$, ppm): δ = -80.8. IR (KBr, cm^{-1}): $\tilde{\upsilon}$ = 3341 (N–H), 1132 (P=O), 996s (P–N).

*[1,3- $(Ph_2P(O)NHCH_2)_2C_6H_4.SnPh_2Cl_2]_n$ (**C_{b7}**)*

Mp: 191-194 °C. ^{1}H NMR ($CDCl_3$, ppm): δ = 3.11 (m, 2H, N–H), 4.09 (m, 4H, CH_2), 6.92–7.93 (m, 48H, Ph-P + Ph-Sn). ^{31}P NMR (CDCl3, ppm): δ =31.5. ^{119}Sn NMR ($CDCl_3$, ppm): δ = low solubility. IR (KBr, cm^{-1}): $\tilde{\upsilon}$ = 3436 (N–H), 1133 (P=O).

*[1,3- $(Ph_2P(O)NHCH_2)_2C_6H_4.SnMe_2Cl_2]_n$ (**C_{c7}**)*

Mp: 196-198 °C. ^{1}H NMR ($CDCl_3$, ppm): δ =1.21 (s, 6H, $^2J(^{119/117}Sn, ^1H)$ = 77.9 Hz, Me-Sn), 3.68 (ps-q, 2H, $^3J_{PH}$ = 6.5 Hz, N–H), 4.11 (ps-t, 4H, $^3J_{PH}$ = 7.5 Hz, CH_2), 7.20–7.27 (m, 8H, Ph), 7.48–7.52 (m, 12H, Ph), 7.80–7.86 (m, 8H, Ph), 7.94 (m, 8H, Ph). ^{31}P NMR (CDCl3, ppm): δ = 26.6. ^{119}Sn NMR ($CDCl_3$, ppm): δ = low solubility. IR (KBr, cm^{-1}): $\tilde{\upsilon}$ = 3318 (m, N–H), 3059, 1146 (s, P=O), 996 (s).

2.4. Crystallography

Single crystal X-ray data of compounds **L_4**, **C_{a3}** and **C_{c5}** was collected on Bruker APEX-II diffractometer with CCD area detector [21] using graphite monochromated Mo-*Ka* radiations (λ= 0.71073 Å) while for **C_{a4}** we used Gemini of Agilent with Atlas CCD detector, mirror-collimated Cu-*Ka* radiation (λ= 1.5418 Å) and software package CrysAlis PRO [22]. The structures were refined by full-matrix least-squares methods against F^2 with *Jana2006* (**C_{a4}**) [23] and *SHELXL-97* (**L_4**, **C_{a3}** and **C_{c5}**) [24]. The

crystallographic and refinement data are summarized in Table 1.

2.5. Statistical analysis for QSAR model

In order to identify the effect of physicochemical parameters on the antibacterial activity, QSAR studies were undertaken using the approach described by Hansch and Fujita [25]. The stepwise multiple linear regression (MLR) procedure is a common method in QSAR studies for selection descriptors. The MLR method performed by the software package SPSS 16.0 was used for selection of the electronic and structural descriptors obtained by the quantum chemical calculations. The electronic descriptors include the energy of frontier orbital (E_{HOMO} and E_{LUMO}), electrophilicity (ω), polarizability (*PL*, the charge difference between the atoms in functional groups) and the net atomic charges (*Q*). Also dipole moment (μ) and molecular volume (*Mv*) are the structural descriptors. E_{HOMO}, E_{LUMO}, ω, *P*, *Q*, μ and *Mv* values are obtained from the DFT results. The toxicities of phosphorhydrazide analogues are expressed in terms of log(1/*MIC*) as an antibacterial activity. The descriptor values were related with activity using MLR analysis. MLR of descriptors, selected for biological activity, gives rise to the problem of multicollinearity. This problem can be solved by using the principal component analysis (PCA) by MINITAB14 software. These linear combinations form a new set of variables, namely principal components (PCs), which are mutually orthogonal. The first PC contains the largest variance and the second new variable contains the second largest variance, and so on. The variable selection in this PCA study was performed by using the Fisher's weights. The descriptors with higher correlation coefficient and lower correlation ($|r|$ <

0.5) to log(1/*MIC*) were selected to carry out stepwise MLR analysis and to optimize the QSAR equation [26]. The stable geometry structures of compounds were further fully optimized using the Density functional theory (DFT).

2.6. Antimicrobial assay

The antibacterial activity of all the compounds was screened *in vitro* against Gram-negative: *E. coli* (ATCC 10553), and Gram-posetive: *B. cereus* (prepared from a teaching microbiological laboratory) bacteria. We used paper broth microdilution method according to the international guideline of the CLSI (Clinical and Laboratory Standard Institute) [27]. Minimum inhibitory concentrations (MIC) for the tested compounds were determined by broth microdilution method. A stock solution of compounds in methanol was prepared and serially twofold diluted using Nutrient Broth to give final concentrations of 0.25-512µg/mL in sterile 96-well microplates. 100 µL of each cell suspension of approximately 10^5 CFU/mL was added into the wells (each containing 100 µL of different concentration of compounds). The maximum percentage of methanol present in the wells was 5% v/v (a control treatment, with all tested bacteria, using 5% methanol showed no antibacterial activity). The MIC, defined as the lowest concentration of the compound which inhibited the visible growth of bacteria, was determined visually after incubation for 24 h at 37 °C. Results were generated from at least three independent experiments, triplicate each. Testes using $SnPh_3Cl$, $SnPh_2Cl_2$, $SnMe_2Cl_2$, $SnPhCl_3$ and gentamicin as positives controls were carried out in parallel [28] (Table 3).

3. Results and discussion

3.1. Synthesis and spectroscopic characterization

The ligands were prepared using the same method from the reaction of $Ph_2P(O)Cl$ with the corresponding diamine (2:1 molar ratio) in presence of Et_3N as HCl scavenger. Among the ligands, suitable crystal of **L_4** for X-ray analysis was obtained from a THF:H_2O solution (2:1). Various solvents were assessed in the crystallization of complexes. However, single crystals of only three complexes were obtained by evaporation from solutions of $HCCl_3$:CH_3OH (1:1), at room temperature and attempts to grow good quality crystals of the other compounds were unsuccessful. All the compounds were characterized by IR and multinuclear NMR spectroscopy. A significant decreasing of the P=O stretching frequencies is observed by ligation of the diphosphoryl ligands. Other prominent bands at 3175-3390 $cm^{-1}$are assigned to N-H vibrational modesthat shift toward higher frequencies in the coordinated ligands. Whereas the N–H bond participates in the hydrogen bonding, the positive shift of υ(N–H) may be attributed to the weakening of the hydrogen bonds from NH…$O_{P=O}$ in NH…Cl of complexes.

NMR spectroscopic results indicated that chemical shift (δ) of ^{31}P for the complexes was almost more up-fielded than those of the corresponding ligands. The integrated ^{1}H NMR spectra of $SnPh_3Cl$ complexes are suggestive of binuclear structures, which exhibit the expected proton signals for a bridging ligands and two triphenyltin(IV). The single resonance at -80.8 to -181.2 ppm in the ^{119}Sn NMR spectra of these compounds provides additional evidence for five-coordinated tin centers in this solution [29]. Since methanol

is a coordinating solvent, binding to Sn and replacing with ligand is also probable. Besides, the ^{119}Sn signal for diorganotin complexes lies (-452.5, -471.5 and -245.5 ppm for $\mathbf{C_{b2}}$, $\mathbf{C_{b3}}$ and $\mathbf{C_{c1}}$, respectively) at higher frequencies which strongly supports the six coordination around the tin centers [30]. The integrated ^{1}H NMR spectra of them are consistent with the formula of 1:1 adducts.

Conclusive information is obtained from the values of the coupling constants, $^{n}J(^{119/117}\text{Sn}, ^{1}\text{H})$ and $^{n}J(^{119/117}\text{Sn}, ^{13}\text{C})$ from the ^{1}H and ^{13}C NMR spectra. The coupling constants $^{2}J(^{119/117}\text{Sn}, ^{13}\text{C})$ and $^{3}J(^{119/117}\text{Sn}, ^{13}\text{C})$ for triphenyltin adducts (40-47 and 60-73 Hz, respectively) lie within the range of five-coordinated species; but the higher values for diphenyltins (48-72 and 86-123 Hz, respectively) indicates the higher coordination number of tin in these complexes. Besides, $^{2}J(^{119/117}\text{Sn}, ^{1}\text{H})$ for dimethyltin(IV) compounds (78-112 Hz) is higher than original $SnMe_2Cl_2$ (68.7 Hz) and falls in the range for six-coordinated dimethyltin(IV) species [31]. In the case of $\mathbf{C_{c5}}$, substitution of $^{2}J(^{119/117}\text{Sn}, ^{1}\text{H})$ Lockhart-Manders [32] equation gives a value of 178.5° for the Me-Sn-Me angle, in accordance with the value in the solid-state structure (168.4°). The other remarkable coupling constant values cannot be extracted from the spectra because of the complexity and overlapping of peaks in the aromatic region (for di- and tri-phenyltin complexes) or disappearing of Me satellites in ^{13}C NMR spectra of low soluble dimethyltin species.

Finally, it should be noted that the integrated ^{1}H NMR spectra of all complexes with $\mathbf{L_6}$ ($\mathbf{C_{a1}}$, $\mathbf{C_{b6}}$ and $\mathbf{C_{d6}}$) are consistent with the formula of binuclear adducts. However, this result is not informative enough to be evidence of the adducts in solution. Although the ^{119}Sn NMR resonance of them shift from the values observed for the parent

organotins(IV), such chemical shifts are not still in the range typical for the five-coordinated tin compounds. This might be a hint that they partially or almost completely dissociated in the solution.

3.2. X-ray crystallography investigation

*3.2.1. Crystal structure of $Ph_2P(O)NMe–(CH_2)_2–NMeP(O)Ph_2$ (**L_4**)*

The structure of **L_4** is shown in (Fig 1a) and the most relevant bond distances are listed in Table 2. The P=O groups are on opposite sides of the molecules. Crystal lattice of **L_4** contains one-dimensional hydrogen-bonded chains along *c*-axis which is produced by the $O\text{-}H_w\ldots O_{P=O}$ interactions. Water molecules, as bifurcated H-donors to P=O groups, build up $R_4^4(8)$ rings between two adjacent diphosphoryl units into the [001] chains (Fig 1b). Weaker CH…O (C3…O1w: 3.357(1) Å, C3-H3: 0.95 Å, ∠C3-H3…O1w: 140°) and CH…π interactions are also the driving force in generating a 3D network in **L_4** (Fig. S1). Similar crystal packing pattern were already observed for the analogous structure of **L_5** including water molecule [17].

*3.2.2. Crystal structure of triphenyl tin(IV) complexes **C_{a3}** and **C_{a4}***

Both of complexes **C_{a3}** and **C_{a4}** crystalize in the monoclinic space group P $2_1/n$ with two symmetry-independent molecules in the unit cell. Fig. 2 and 3 shows an ORTEP representation of the molecular structures for these complexes, and selected bond distances and angles are listed in Table 2. The complexes have a binuclear structure, with centrosymmetric bridging molecules of the diphosphoryl ligand and tin moieties.

The central tin atoms are in trigonal–bipyramidal environments formed by three phenyl groups in the equatorial plane, one chloride ion and the phosphoryl group in the apical (*trans*) positions. The *trans* angles around tin are 179.07(9)° and 177.51(3)°, and the sum of angles in the trigonal girdle around Sn are 357.40° and 358.94° (for $\mathbf{C_{a3}}$ and $\mathbf{C_{a4}}$, respectively.

The Sn–C bond distances (Table 2) are in a good agreement with the published values [15, 17]. These values also correspond well with the sum of the covalent radii (2.15 Å) of tin and carbon [33]. The Sn–Cl bond lengths are 2.5075(9) and 2.5000(5) Å (in $\mathbf{C_{a3}}$ and $\mathbf{C_{a4}}$, respectively), lying in the normal covalent radii 2.37–2.60 Å while the Sn–O bonds (2.363(2) and 2.3258(12) Å in $\mathbf{C_{a3}}$ and $\mathbf{C_{a4}}$, respectively) are in accordance with the coordinate bond. A comparison between the crystal structures of $\mathbf{C_{a4}}$ and its ligand, $\mathbf{L_4}$, reveals that by coordinating the ligand to Sn, the P=O bond gets longer (about 0.013 Å). Lengthening of the P=O bond is simply described by polarization of the phosphoryl group in the electrostatic field of the tin(IV) atom. In return, the P-N and P-C bonds are shortened about 0.011 Å in the complex $\mathbf{C_{a4}}$ (Table 2).

The crystal structure of $\mathbf{C_{a4}}$ is governed by CH…Cl interactions which build up a 3D network. Here, the chlorine atom acts as a trifurcated acceptor involved in hydrogen bonding with ligand-bound Ph rings of other molecular units (Fig. S2). These non-classic hydrogen bonds are established in this compound with different donor–acceptor distances of 3.5677(18) (C21H21…Cl1), 3.708(2) (C28H28…Cl1) and 3.768(2) Å (C22H22…Cl1).

In contrast, the presence of N–H moieties in $\mathbf{C_{a3}}$ leads to the formation of interesting inter-molecular hydrogen bonding. Each molecule of the complex is associated with other

four molecules through symmetry-equivalent NH…Cl linkages (N…Cl: 3.664(3) Å, N-H: 0.86 Å, ∠N-H…Cl: 148°) in a two-dimensional arrangement (Fig. S3). Besides, the crystal packing of $\mathbf{C_{a3}}$ is further stabilized by weaker intermolecular C-H…π interactions between hydrogen-bonded neighboring complexes.

3.2.3. Crystal structure of dimethyl tin(IV) complex $\boldsymbol{C_{a5}}$

In the crystalline state, the title complex adopts an infinite zigzag chain structure which is produced by the bidentate bridging diphosphoryl ligand and the Sn(IV) center. As shown in Fig. 4, each central tin atom is surrounded by two carbon, two chlorine and two oxygen atoms in a *trans-cis* octahedral geometry. The *trans* bond angles around the Sn(IV) centers are 168.37(5) (∠C1–Sn1–C2), 169.53(2) (∠O1–Sn1–Cl1) and 175.94(2)° (∠O2–Sn1–Cl2), indicating a distortion of the geometry. The *cis* bond angles are in the range of 87.23(4) (∠C2–Sn1–O1) to 98.30(4)° (∠C1–Sn1)–Cl1) and deviate from the idealized value (90°), close to the reported values for other *trans–cis* dimethyltin(IV) adducts [31].

As usually, the methyl groups are in *trans* positions with almost equal distances (Table 2). Non-symmetrical coordination of the bidentate O2-ligand to tin can be observed with two different Sn–O distances (2.3486(10) and 2.2718(10) Å) and also two different P–O–Sn angles (163.35(5) and 149.66(5)°, respectively). There are chlorine atoms in *trans* position of the two oxygen atoms and distances are correlated: the shorter is Sn–O, the longer is Sn–Cl (*trans* effect), in agreement with other organotin phosphoramidates [34]. The P=O bond distances of 2.5006(9) and 2.5030(9) A are in the range found for P–O-

single bonds in other phosphoryl compounds, indicating a considerable lengthening of the P=O bond by (P–O→Sn) coordination.

As mentioned earlier, Sn-O interactions have a substantial contribution to the organization and stabilization of the crystal structure. 1D infinite coordination chains extend in the crystallographic *b*-direction with Sn-Sn separation of 10.529 Å. The neighboring chains are correlated by CH…Cl interactions (C14H14…Cl2: 3.606(2) Å and C5H5…Cl1: 3.606(2) Å along *c* axis and C26H26…Cl1: 3.606(2) Å in *a*-direction), generating a 3D network (Fig S4).

3.5. Bioassay

Broth microdilution susceptibility tests were conducted to evaluate the antibacterial activity of tin complexes and the corresponding ligands. Two Gram-negative (*E. coli*) and Gram-posetive (*B. cereus*) was examined. To substantiate the results, tests were carried out for $SnPh_3Cl$, $SnPh_2Cl_2$, $SnPhCl_3$, $SnMe_2Cl_2$ and the commercial antibiotic gentamicin as positive controls. The MIC values (μg/mL) are presented in Table 3. Based on the MIC test, the ligands are devoid of antibacterial activity. Notably, among the compounds, triphenyltin complexes exhibited **a** marked activity only against Gram-positive bacterium *B. Cereus* (IC_{50} = 0.78 μg/mL for $\mathbf{C_{a3}}$ and $\mathbf{C_{a5}}$). In addition, the antibacterial activity of $\mathbf{C_{a3}}$ and $\mathbf{C_{a5}}$ exceeded those of the primary compounds $SnPh_2Cl_2$, $SnPhCl_3$ and $SnMe_2Cl_2$. Besides, the antibacterial activity of gentamicin was higher than that of $\mathbf{C_{a3}}$ and $\mathbf{C_{a5}}$ (Table 3). Literature survey reveals that Sn complexes have a variety of remarkable antimicrobial potencies, although mode of action and mechanism has not been clarified

yet. Three possible mechanisms for biocidal ability of aqueous Sn ions can be distinguished: (i) binding to bacterial enzymes and inhibiting them from their functions, (ii) binding to bacterial DNA and leading to inhibition of cell replication, and (iii) interaction with the cell membrane of the bacteria and ultimately causing cell death [35]. To gain a better understanding of the inhibitory potential of the synthesized complexes and to study on their mechanism in more detail, it was necessary to examine the interaction of the derivatives with the bacterial structures by QSAR method. QSAR technique was used to find the effective electronic and structural parameters.

3.6. QSAR analysis

According to Hansch and his co-workers, there is a relationship between the physico-chemical properties of a molecule, mainly electronic, steric and hydrophobic factors, and its biological activity. In our previous works, the QSAR studies have been performed on some bisphosphoramide compounds relating to their anticholineaterase activities, and showed that the electronic properties are closely correlated with biological potency of the studied compounds. Here, with Sn complexes attached to phosphorus atoms of bisphosphoramide ligand, we used quantum chemical calculations in order to obtain electronic and structural properties of the complexes, to see if such correlation is also valid. QSAR studies were done in order to recognize the effect of descriptors on the activity of bacterial. The stepwise MLR procedure was used for model selection, which is a common method used in QSAR studies.

To obtain the electronic and structural descriptors given in Table 4, we used the optimization structures to calculate by the level of B3LYP/LANL2DZ and 6-311G* basis set in the water solvent used for all molecules. Using the descriptors from Table 4, the following equation was obtained:

$$\log(1/\mathrm{MIC}) = -15.543Q_P - 7.156Q_O + 4.262Q_N + 0.016PL_{P-O} - 10.092PL_{Sn-O} + 46.963E_{HOMO} + 944.0331E_{LUMO} + 545.572\omega + 0.193\mu + 0.002Mv - 61.187 \quad (2)$$

$$n = 12; R^2 = 0.996; S_{reg} = 0.080; r = 0.146; F_{\text{statistic}} = 28.049$$

Where, n is the number of compounds, r is the correlation coefficient (sig.), R^2 is the determination coefficient, S_{reg} is the standard deviation of regression and $F_{\text{statistic}}$ is the Fisher statistic [36]. The high values of Variance Inflation Factor (VIF >10) caused impossibility to calculate MIC. The best way to deal with such a problem is to calculate variance inflation factor (VIF). We calculated VIF, which is a measure of multicollinearity, for each of the parameters involved in models. The VIF is defined as $1/(1-R_i^2)$, where R_i is the multiple correlation coefficient of the ith independent variable on all of the other independent variables. A VIF 10 or more (no upper limit is defined) for large data sets indicates a collinearity problem. For small data sets, even VIFs of five or more (here also no upper limit is defined) can indicate collinearity. Therefore, the variables with a high VIF are candidates for exclusion from the model [37]. To clarify this problem the PCA method must be used. Fisher's weight approach is a method for the reduction and selection of the best descriptors, which have high correlation between the variables and principal components. PC eqs. 3a and 3b were obtained with eight variables from among seventeen descriptors:

$$PC_1 = +0.254Q_{Sn} + 0.390Q_P + 0.463Q_O - 0.014PL_{P=O} - 0.143PL_{Sn-O} + 0.483E_{LUMO} - 0.476\omega + 0.057Mv \quad (3a)$$

$$PC_2 = +0.512Q_{Sn} - 0.231Q_P + 0.108Q_O + 0.392PL_{P=O} + 0.556PL_{Sn-O} - 0.007E_{LUMO} - 0.029\omega - 0.335Mv \quad (3b)$$

The main variables were found from the principle scores of the normalized eigenvalue of the two principal components. The results showed that the first and second factor PC on the total variance 37.2% and 23.6%, respectively. Then, the new MLR was performed using these eight descriptors (Q_{Sn}, Q_P, Q_O, $PL_{P=O}$, PL_{Sn-O}, E_{LUMO}, ω and Mv) which resulted following equation:

$$\log(1/\text{MIC}) = -38.509Q_{Sn} - 14.844Q_P + 0.767Q_O - 0.051PL_{P-O} - 9.323PL_{Sn-O} + 725.846E_{LUMO} + 406.202\omega + 0.001Mv + 55.304 \quad (4)$$

$$n = 12; R^2 = 0.762; S_{reg} = 0.329; r = 0.289; F_{\text{statistic}} = 1.845$$

The low determination coefficient (R^2 = 0.762 and F = 1.845) with high Variance Inflation Factor (VIF) > 10 (Table 5) indicated the multicollinearity problem. The improvement in the eq. 4 was carried out by omitting the compounds $\mathbf{C_{b3}}$ and $\mathbf{C_{b4}}$ from tested compounds and replacing the Q_{Sn} with Q_P and Q_O as well as ω with E_{LUMO}. Multiple regressions performed using these six parameters yielded the following model with increasing the R^2 = 0.832 and decreasing the S_{reg} = 0.257.

$$\log(1/\text{MIC}) = -14.093Q_{Sn} + 0.032PL_{P-O} + 14.109PL_{Sn-O} - 33.098\omega + 0.001Mv - 11.849 \quad (5)$$

$$n = 10; R^2 = 0.832; S_{reg} = 0.257; r = 0.103; F_{\text{statistic}} = 3.971$$

The correlating parameters have VIF<10, thus there is no colinearity problem (Table 5). In this equation, the inhibitory potency of *B. Cereus* is influenced mainly by the

electronic parameters with preferential order as ω > Q_{Sn} > $PL_{Sn\text{-}O}$ > $PL_{P=O}$ versus structural descriptor (*Mv*). Comparison of the correlation coefficient of ω (-33.098) with random error (-11.849) demonstrates that ω can play a crucial function in the interaction of the complexes with *B. Cereus*. The positive sing of ω in $\log(1/MIC)$ disclose that the compound with higher electropilicity (ω)is indicative of higher activity against bacterial. The correlation matrix was used to determine the interrelationship between the independent variables (Table 6). As shown in Table 6, the majority of regression coefficients were closely correlated. Therefore, orthogonalization of the molecular descriptors was conducted. Orthogonalization of molecular descriptors is undertaken to avoid collinearity among variables and model overfitting. The high interrelationships were observed between ω and Q_{Sn} (r = –0.514), and Q_{Sn} and PL_{Sn-O} (r = +0.660), respectively. A result was obtained from the above data; the electrophilicity parameter controls the influence of the net charge and polarizability of Sn atom of complexes in inhibition of *B. Cereus*.

4. Conclusions

In this work, $SnPh_nCl_{4-n}$ (n=1-3) and $SnMe_2Cl_2$ adducts with a family of diphosphoryl ligands, $(Ph)_2P(O)–X–P(O)(Ph)_2$, have been introduced. The prepared compounds have been characterized by IR and multinuclear NMR spectroscopy. X-Ray crystallography confirms the bridging ligands produce binuclear structures with $SnPh_3Cl$ acceptors and offer 1D polymeric arrangement toward $SnMe_2Cl_2$. The analysis of the crystal packing reveals non-covalent interactions, including Sn-O bonds (in $\mathbf{C_{c5}}$), NH…Cl and CH…Cl

interactions, to be the main factor governing the supramolecular assembly of the crystalline complexes. The synthesized compounds were screened for the antibacterial activity against *B. cereus* and *E. coli*. DFT–QSAR models revealed that the descriptor of the electrophilicity (ω) is related with the inhibition of *B. cereus*. The correlation matrix of QSAR models and docking analysis confirmed that the electrophilicity parameter controls the influence of the net charge (Q_{Sn}) and polarizability of Sn atom of complexes in inhibition of *B. cereus*.

Acknowledgment

The financial support of Tarbiat Modares University's Research Council and the project 14-03276S of the Czech Science Foundation are gratefully acknowledged.

Appendix A. Supplementary material

Crystallographic data for the structural analysis has been deposited with the Cambridge Crystallographic Data Center, CCDC No. 1027074, 1027642, 1027641 and 1027071 for **L_4**, **C_{a3}**, **C_{a4}** and **C_{c5}**, respectively. These data can be obtained free of charge via http://www.ccdc.cam.ac.uk/conts/retrieving.html, or from the Cambridge Crystallographic Data Centre, 12 Union Road, Cambridge CB2 1EZ, UK; fax: (+44) 1223-336-033; or e-mail: deposit@ccdc.cam.ac.uk.

References

[1] T. Wu, M. He, X. Zang, Y. Zhou, T. Qiu, S. Pan, X. Xu, Biochim. Biophys. Acta 1828 (2013) 2751–2756.

[2] X. Shang, X. Meng, E. C.B.A. Alegria, Q. Li, M.F. C. Guedes da Silva, M. L. Kuznetsov, A. J.L. Pombeiro, Inorg. Chem. 50 (2011) 8158-8167.

[3] E. López-Torres, F. Zani, M. A. Mendiola, J. Inorg. Biochem. 105 (2011) 600-608.

[4] (a) T. Sedaghat, M. Naseh, H.R. Khavasi, H. Motamedi, Polyhedron 33 (2012) 435–440. (b) T. S. Basu Baul Appl. Organometal. Chem. 22 (2008) 195–204.

[5] Tin Chemistry: Fundamentals, Frontiers, and Applications, Wrackmeyer, B. in: A. G. Davies, M. Gielen, K. H. Pannell, E. R. T. Tiekink, Wiley, Chichester, UK, 2008, Chapter 2.

[6] *Chemistry of Tin*, 2nd ed.; P. J. Smith, Ed.; Blackie Academic & Professional: London, 1998.

[7] L. Pellerito, L. Nagy, *Coord. Chem. Rev.* **2002**, *224*, 111-150.

[8] C. Pellerito, L. Nagy, L. Pellerito, A. Szorcsik, J. Organomet. Chem. 691 (2006) 1733–1747.

[9] A.A. Soderholm, P.T. Lehtovuori, T.H. Nyronen, J. Med. Chem. 48 (2005) 917–925.

[10] W. Sippl, J. Comput. Aid. Mol. Des. 16 (2002) 825–830.

[11] F. Li,; H. Wua, L. Li, X. Li, J. Zhao, W.G.M. Peijnenburg, Ecotoxi. Envir. Saf. 80 (2012) 273–279.

[12] E.B. De melo, Europ. J. Med. Chem. 45 (2010) 5817–5826.

[13] N.C.Y. Wang, R. Venkatapathy, R.M. Bruce, C. Moudgal, Regul. Toxic. Pharm. 59 (2011) 215–226.

[14] K. Gholivand, S. Farshadian, Z. Hosseini, *J. Organomet Chem.* **2012**, *696*, 4298-4308.

[15] K. Gholivand, A. Gholami, S. K. Tizhoush, K. J. Schenk, F. T. Fadaei, A. Bahrami, *RSC Adv.* **2014**, *4*, 44509-44516.

[16] K. Gholivand, F. Molaei, M. Rajabi, M. D. Esrafili, M. Hosseini, *Polyhedron* **2014**, *71*, 8-16.

[17] K. Gholivand, A. Gholami, A. A. V. Ebrahimi, S. T. Abolghasemi, F. T. Fadaei, K. J. Schenk, M. D. Esrafili, *RSC Adv.* **2015**, *5*, 17482-17492.

[18] M. Rajabi, K. Gholivand, R. Salami, F. Molaei, J. Thibonnet, K. Zare, F. Fadaei T., K. J. Schenk, Inorganica Chimica Acta 432 (2015) 149–157

[19] M.J. Frisch, G.W. Trucks, H.B. Schlegel, G.E. Scuseria, M.A. Robb, J.R. Cheeseman, J.A. Montgomery Jr., T. Vreven, K.N. Kudin, J.C. Burant, J.M. Millam, S.S. Iyengar, J. Tomasi, V. Barone, B. Mennucci, M. Cossi, G. Scalmani, N. Rega, G.A. Petersson, H. Nakatsuji, M. Hada, M. Ehara, K.

Toyota, R. Fukuda, J. Hasegawa, M. Ishida, T. Nakajima, Y. Honda, O. Kitao, H. Nakai, M. Klene, X. Li, J.E. Knox, H.P. Hratchian, J.B. Cross, V. Bakken, C. Adamo, J. Jaramillo, R. Gomperts, R.E. Stratmann, O. Yazyev, A.J. Austin, R. Cammi, C. Pomelli, J.W. Ochterski, P.Y. Ayala, K. Morokuma, G.A. Voth, P. Salvador, J.J. Dannenberg, V.G. Zakrzewski, S. Dapprich, A.D. Daniels, M.C. Strain, O. Farkas, D.K. Malick, A.D. Rabuck, K. Raghavachari, J.B. Foresman, J.V. Ortiz, Q. Cui, A.G. Baboul, S. Clifford, J. Cioslowski, B.B. Stefanov, G. Liu, A. Liashenko, P. Piskorz, I. Komaromi, R.L. Martin, D.J. Fox, T. Keith, M.A. Al-Laham, C.Y. Peng, A. Nanayakkara, M. Challacombe, P.M.W. Gill, B. Johnson, W. Chen, M.W. Wong, C. Gonzalez, J.A. Pople, Gaussian 03, Revision D.01, Gaussian, Inc., Wallingford CT, 2005.

[20] SPSS for Windows, Version 10.05, SPSS Inc., Bangalore, India, 1999.

[21] Bruker, Programs APEX II, version 2.0–1; SAINT, version 7.23A; SADABS, version 2004/1; XPREP, version 2005/2; SHELXTL, version 6.1. Bruker AXS Inc., Madison, WI, USA, 2005.

[22] Agilent Technologies CrysAlis PRO, Yarnton, Oxfordshire, UK, 2010.

[23] V. Petricek, M. Dusek, L. Palatinus, Z. Kristallogr. 229(5) (2014) 345-352.

[24] G.M. Sheldrick, Acta. Cryst. A. 64 (2008) 112–122.

[25] C. Hansch, T. Fujita, J. Am. Chem. Soc. 86 (1964**)** 1616–1626.

[26] K. De, C. Sengupta, K. Roy, Bioorg. Med. Chem. 12 (2004**)** 3323–3332.

[27] Performance standards for antimicrobial susceptibility testing; 21st informational supplement. CLSI document M100-S21. Clinical and Laboratory Standards Institute, 940 West Valley Road, Suite 1400, Wayne, Pennsylvania 19087, USA, 2011.

[28] J.M. Andrews, J. Antimicrob. Chemother. 48 (2001) 5–16.

[29] (a) C. H. Yoder, L. A. Margolis and J. M. Horne, J. Organomet. Chem. 633 **(**2001) 33-38. (b) M. Nádvorník, J. Holeček, K. Handlíř and A. Lyčka, *J. Organomet. Chem.* 275 (1984) 43-51.

[30] J. Holecek, M. Nadvornik, K. Handlir, A. Lycka, J. Organomet. Chem. 315 **(**1986) 299–308.

[31] K. Gholivand, S. Farshadian, Inorg. Chim. Acta 368 (2011) 111-123.

[32] T. P. Lockhart, W. F. Manders, Inorg. Chem. 25 (1986) 892-895.

[33] A. Bondi, J. Phys. Chem. 68 **(**1964) 441–451.

[34] A.R. Narga, M. Schuermann, C. Silvestru, J. Organomet. Chem. 623 **(**2001) 161–167.

[35] B. Coyle, K. Kavanagh, M. McCann, M. Devereux, M. Geraghty, BioMetals 16 (2003) 321–329.

[36] D.R. Roy, U. Sarkar, P.K. Chattaraj, A. Mitra, J. Padmanabhan, R. Parthasarathi, V. Subramanian, S. Van Damme, P. Bultinck, Mol. Divers. 10 (2006) 119–131.

[37] J. Singh, B. Shaik, S. Singh, V.K. Agrawal, P.V. Khadikar, O. Deeb, C.T. Supuran, Chem. Biol. Drug. Des. 71 (2008) 244–259.

Figure Captions

Fig. 1. (a) General view of $\mathbf{L_4}$ in representation of atoms via thermal ellipsoids at 50% probability level. **(b)** Illustration of $R_4^4(8)$ graph set in $\mathbf{L_4}$

Fig. 2. General view of $\mathbf{C_{a3}}$ with numbering non-carbon atoms (at 50% probability level). Hydrogen atoms omitted for clarity. Only major parts of disordered fragments are shown.

Fig. 3. General view of $\mathbf{C_{a4}}$ with numbering non-carbon atoms (at 50% probability level). Hydrogen atoms omitted for clarity.

Fig 4. (a) Independent part of unit cell for $\mathbf{C_{c5}}$. Atoms are represented by thermal displacement ellipsoids, p=50%. Hydrogen atoms omitted for clarity. **(b)** The polymeric structure in the crystal.

Scheme 1. Preparation pathway of organotin(IV) diphosphoramidates

Table 1 Crystallographic data of compounds $\mathbf{L_4}$, $\mathbf{C_{a3}}$ and $\mathbf{C_{a4}}$

Forms	$\mathbf{L_4}$	$\mathbf{C_{a3}}$	$\mathbf{C_{a4}}$	$\mathbf{C_{c5}}$
Empirical formula	C28H34N2O4P2	C64H60Cl2N2O2P2Sn2	C64H60Cl2N2O2P2Sn2	$C_{30}H_{34}Cl_2N_2O_2P_2Sn$
Formula weight	524.51	1259.36	1259.5	706.12
Temperature (K)	100(2)	100(2)	120.00	100
Wavelength (Å)	0.71073	0.71073	1.5418	monoclinic
Crystal system, space group	Monoclinic, $P2_1/n$	Monoclinic, $P2_1/n$	Monoclinic, $P2_1/n$	$P2_1/n$
Unit cell dimensions				
a (Å)	9.0657(3)	11.3006(4)	18.2825(8)	9.844(3)
b (Å)	15.2603(5)	19.9203(7)	9.2659(3)	19.667(7)
c (Å)	10.1751(3)	12.6655(4)	19.0782(8)	16.031(5)
α (°)	90	90	90	90.00
β (°)	110.086(10)	95.7370(10)	117.151(4)	100.247(13)
γ (°)	90	90	90	90.00
V (Å^3)	1322.06(7)	2836.87(17)	2875.8(2)	3054.0(18)
Z, Calculated density (Mg.m^{-3})	2, 1.318	2, 1.474	2, 1.454	4, 1.536
Absorption coefficient (mm^{-1})	0.202	1.077	8.637	1.147
F(000)	556	1276	1276	1432.0
Crystal size (mm^3)	0.21×0.17×0.13	0.260×0.050×0.050	0.311×0.295×0.050	0.24 × 0.22 × 0.21
θ range for data collection (°)	2.51–29.00	1.91–30.00	4.54–67.11	3.3 to 64.06
Limiting indices	-12≤h≤12 -20≤k≤20, -13≤l≤13	-15≤h≤15 -27≤k≤28 -17≤l≤17	-21≤h≤20 -7≤k≤10 -18≤l≤22	-14 ≤ h ≤ 14 -29 ≤ k ≤ 29 -23 ≤ l ≤ 23
Reflections collected / unique	15564/3515 (0.0187)	37314/8277 (0.0405)	10787/4128 (0.0343)	45138
Completeness to theta	100.0%	100.0%	98%	100.0%
Absorption correction	Semi-empirical from equivalents	Semi-empirical from equivalents	Semi-empirical from equivalents	Semi-empirical from equivalents
Refinement method	Full-matrix least-squares on F^2	Full-matrix least-squares on F^2	Full-matrix least-squares on F^2	Full-matrix least-squares on F^2
Data/restraints/parameters	3515/0/166	8277/0/335	5008/0/344	10635/0/354
Goodness-of-fit on F^2	1.054	1.009	1.27	1.045
Final R indices	R_1 = 0.0311, wR_2 = 0.0838	R_1 = 0.0265, wR_2 = 0.0562	R_1 = 0.0319, wR_2 = 0.0858	R_1 = 0.0195, wR_2 = 0.0486
R indices (all data)	R_1 = 0.0353, wR_2 = 0.0878	R_1 = 0.0391, wR_2 = 0.0600	R_1 = 0.0413, wR_2 = 0.0930	R_1 = 0.0225, wR_2 = 0.0503
Largest diff. peak and hole (e.Å^{-3})	0.471 and -0.285	0.662 and -0.555	0.50 and -0.56	0.62 and -0.47

Table 2 Selected bond lengths (Å) and angles (°) for crystalline compounds $\mathbf{L_4}$, $\mathbf{C_{a3}}$ and $\mathbf{C_{a4}}$.

	***d*(P-C)**	***d*(P-N)**	***d*(P=O)**	***d*(Sn-O)**	***d*(Sn-Cl)**	***d*(Sn-C)**	**∠P-O-Sn**	**∠O-Sn-Cl**	**∠C-Sn-C**
$\mathbf{L_4}$	1.7990(14) 1.8048(15)	1.6571(13)	1.4974(11)	-	-	-		-	-
$\mathbf{C_{a3}}$	1.801(4) 1.804(4)	1.625(4)	1.496(2)	2.363(2)	2.5075(9)	2.076(12) 2.134(5) 2.119(4)	170.6(2)	179.07(9)	117.3(6) 118.15(16) 122.0(7)
$\mathbf{C_{a4}}$	1.7875(18) 1.7998(18)	1.6419(15)	1.5091(12)	2.3258(12)	2.5000(5)	2.1363(18) 2.1377(18) 2.1383(17)	140.06(7)	177.51(3)	118.06(7) 120.14(7) 120.74(7)
$\mathbf{C_{c5}}$	1.8012(13) 1.8019(12) 1.7922(13) 1.8021(13)	1.6682(11) 1.6445(10)	2.5006(9) 2.5030(9)	2.3486(10) 2.2718(10)	2.4851(7) 2.5258(7)	2.1213(12) 2.1246(12)	163.35(5) 149.66(5)	169.53(2) 175.94(2)	168.37(5)

Table 3. Minimum Inhibitory Concentration (MIC[a], *μg/mL*) as a criterion of antibacterial activities of the synthesized compounds.

Compound	*B. Cereus*	*E. Coli*
$\mathbf{C_{a1}}$	25.0	----
$\mathbf{C_{b1}}$	----[b]	10.0
$\mathbf{C_{c1}}$	10.0	----
$\mathbf{C_{a2}}$	1.50	----
$\mathbf{C_{b2}}$	6.00	5.00
$\mathbf{C_{c2}}$	5.00	----
$\mathbf{C_{a3}}$	0.78	----
$\mathbf{C_{b3}}$	12.0	10.0
$\mathbf{C_{c3}}$	10.0	----
$\mathbf{C_{a4}}$	12.0	----
$\mathbf{C_{b4}}$	3.00	5.00
$\mathbf{C_{a5}}$	0.78	----
$\mathbf{C_{b5}}$	6.00	2.50
$\mathbf{C_{c5}}$	10.0	----
$\mathbf{C_{a6}}$	1.50	----
$\mathbf{C_{b6}}$	12.0	5.00
$\mathbf{C_{c6}}$	----	10.0
$\mathbf{C_{a7}}$	1.50	----
$\mathbf{C_{b7}}$	6.00	5.00
$\mathbf{C_{d7}}$	10.0	----
$\mathbf{SnPh_3Cl}$	0.78	----
$\mathbf{SnPh_2Cl_2}$	3.00	25.0
$\mathbf{SnPhCl_3}$	6.00	10.0
$\mathbf{SnMe_2Cl_2}$	25.0	10.0
Gentamicin	0.12	0.50

[a] minimal inhibitory concentration (MIC) observed after 24 h of incubation at 37 °C; [b] not tested.

Table 4. Quantum–chemical and geometrical descriptors for title compounds computed at B3LYP/6–311G* level

No.	Electronic descriptors										Structural descriptors	
	Charge				Polarizability			Frontier molecular orbital			Lipophilicity	Steric
	Q_{Sn} (a.u)	Q_P (a.u)	Q_O (a.u)	Q_N (a.u)	PL_{P-O}	PL_{N-H}	PL_{Sn-O}	E_{HOMO}	E_{LUMO}	ω	μ (Debye)	Mv (cm^3/mol)
C1	2.165	2.088	-1.152	-0.992	-3.240	1.404	3.317	-0.249	-0.071	0.143	0.0010	----
C2	2.119	2.089	-1.163	-0.994	-3.252	1.404	3.282	-0.260	-0.077	0.155	0.0006	612.370
C3	2.091	2.118	-1.176	-1.053	-3.294	1.488	3.267	-0.257	-0.079	0.158	1.6791	831.821
C4	2.165	2.078	-1.142	-0.994	-3.229	1.400	3.307	-0.238	-0.059	0.123	0.9622	765.620
C5	2.137	2.094	-1.181	-0.994	-3.275	1.399	3.318	-0.248	-0.073	0.147	1.4838	619.466
C6	2.096	2.116	-1.182	-1.040	-3.298	1.472	3.278	-0.248	-0.071	0.144	1.0469	1077.262
C7	2.165	2.085	-1.150	-0.996	-3.236	1.397	3.315	-0.239	-0.055	0.117	1.1510	831.430
C8	2.132	2.097	-1.182	-0.993	-3.279	1.339	3.314	-0.253	-0.067	0.137	0.0007	639.636
C9	2.097	2.119	-1.182	-1.039	-3.301	-1.470	3.279	-0.243	-0.077	0.154	0.0007	1086.365
C10	2.165	2.119	-1.161	-0.864	-3.280	----[a]	3.326	-0.247	-0.074	0.149	-----	812.431
C11	2.122	2.122	-1.177	-0.859	-3.299	----	3.299	-0.258	-0.078	0.157	0.0015	767.786
C12	2.089	2.131	-1.168	-0.876	-3.301	----	-3.257	-0.248	-0.073	0.147	0.0006	----
C13	2.174	2.113	-1.148	-0.865	3.271	----	3.324	-0.248	-0.070	0.142	0.6245	875.247
C14	2.132	2.119	-1.175	-0.869	-3.294	----	3.307	-0.256	-0.071	0.144	0.0024	977.050
C15	2.089	2.099	-1.181	-0.870	-3.280	----	3.270	-0.247	-0.065	0.133	0.0002	861.683
C16	2.112	2.188	-1.149	----	-3.337	----	3.261	-0.254	-0.065	0.134	0.0031	697.538
C18	2.147	2.511	-1.105	-1.005	-3.616	-1.408	3.252	-0.246	-0.033	0.091	0.0000	932.621

[a] ---- = Not tested due to insufficient quantities

Table 5 VIF[a] values for the QSAR equations

Independent variable	*B. cereus*		
	Eq. (2)	**Eq. (4)**	**Eq. (5)**
Q_{Sn}		9.745	12.429
Q_P	145.677	135.329	
Q_O	14.422	11.003	
Q_N	3.113		
$PL_{P=O}$	4.016	3.525	2.120
PL_{Sn-O}	3.671	3.400	7.195
E_{HOMO}	4.520		
E_{LUMO}	6.668	5.944	
ω	5.152	4.514	6.856
μ	2.621		
Mv	2.145	1.748	1.386

[a] VIF = $1/(1-R_i^2)$; where, R_i is the multiple correlation coefficient of the *ith* independent variable on all of the other independent variables.

Table 6 Correlation matrix for the antibacterial properties and the selected variables in Eq. (5).

Selected variables	*B. cereus*				
	Q_{Sn}	$PL_{P=O}$	PL_{Sn-O}	ω	Mv
Q_{Sn}	1.000				
$PL_{P=O}$	0.463	1.000			
PL_{Sn-O}	0.660	0.480	1.000		
ω	-0.514	0.149	0.204	1.000	
Mv	-0.409	-0.038	-0.442	0.088	1.000

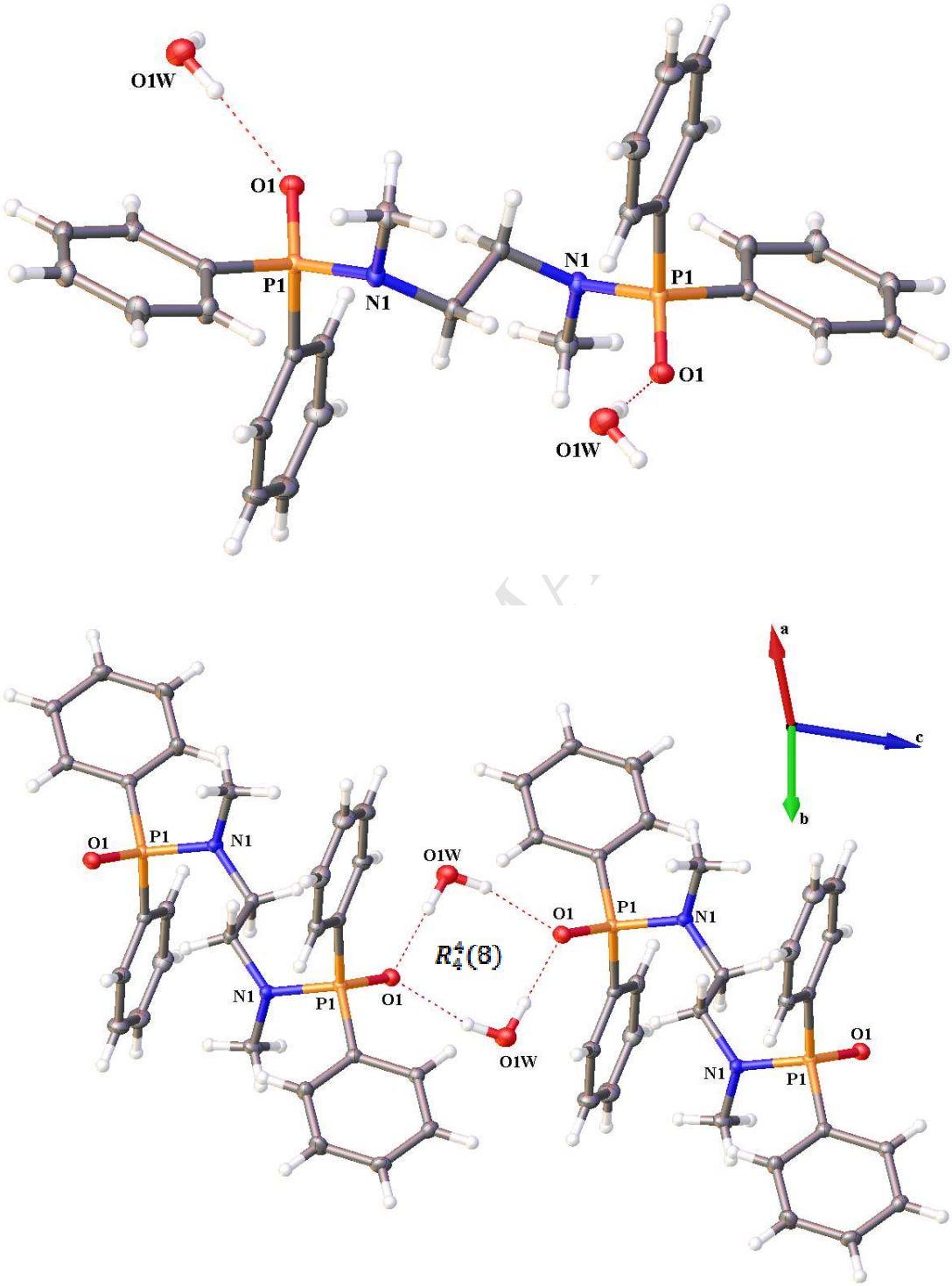
O1W
O1
P1
N1
N1
P1
O1
O1W
a
c
b
O1
P1
N1
O1W
O1
P1
N1
$R_4^4(8)$
N1
P1
O1
O1W
N1
P1
O1

Fig. 1

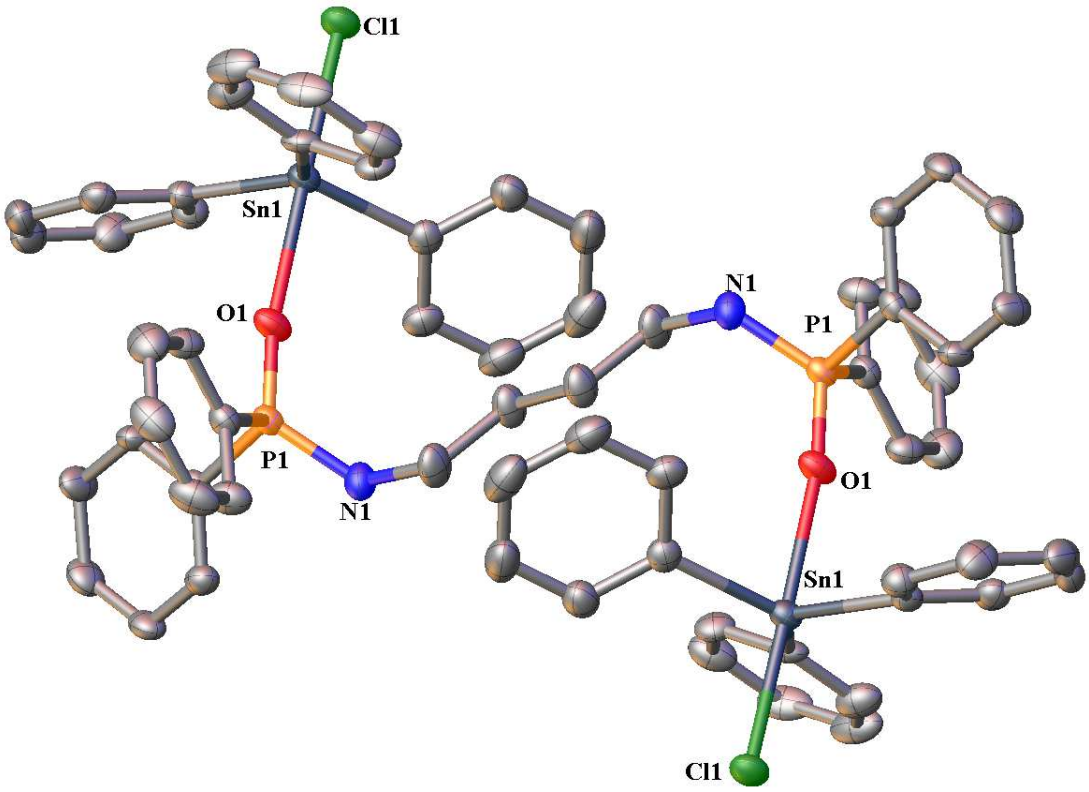

Fig. 2

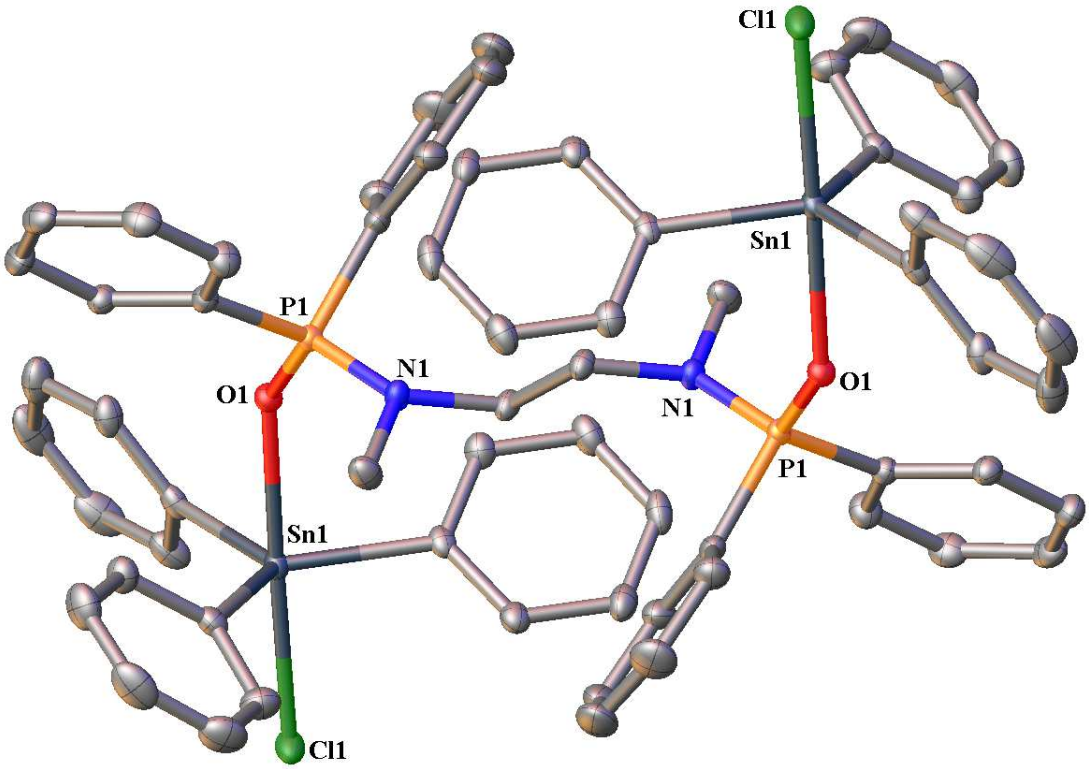

Fig. 3

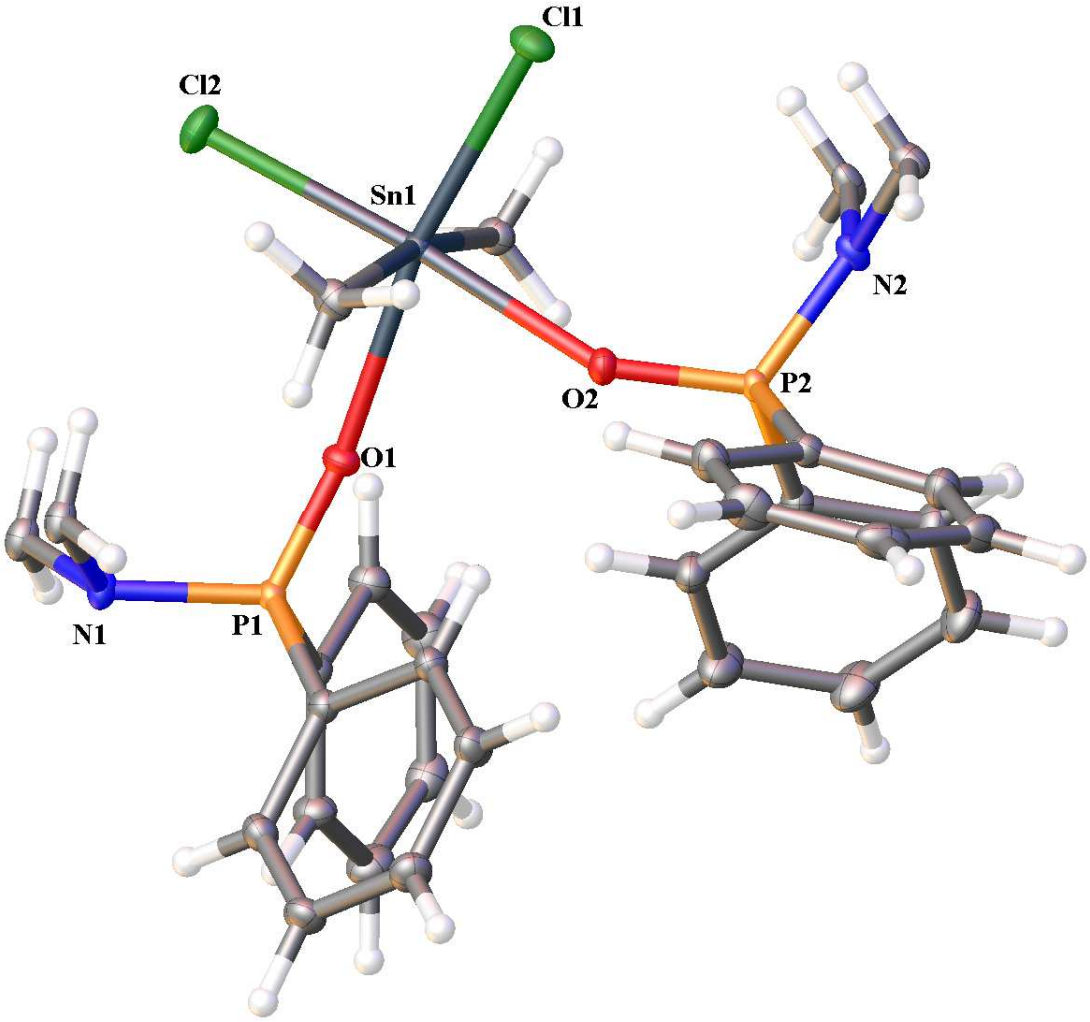

Fig. 4a

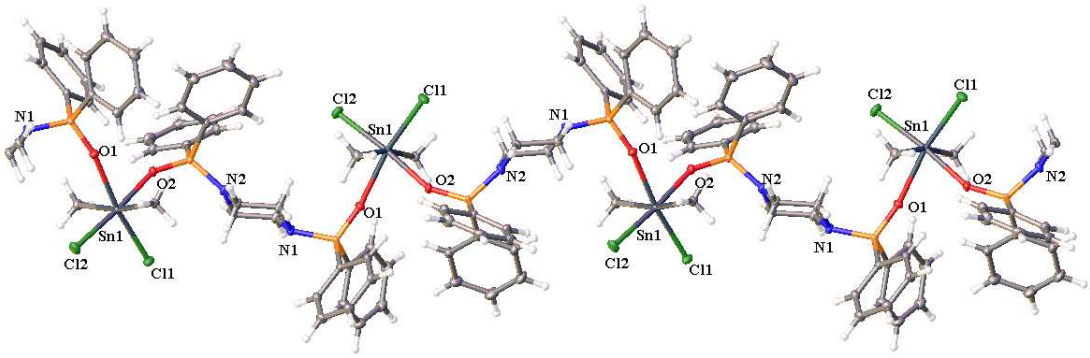

Fig. 4b

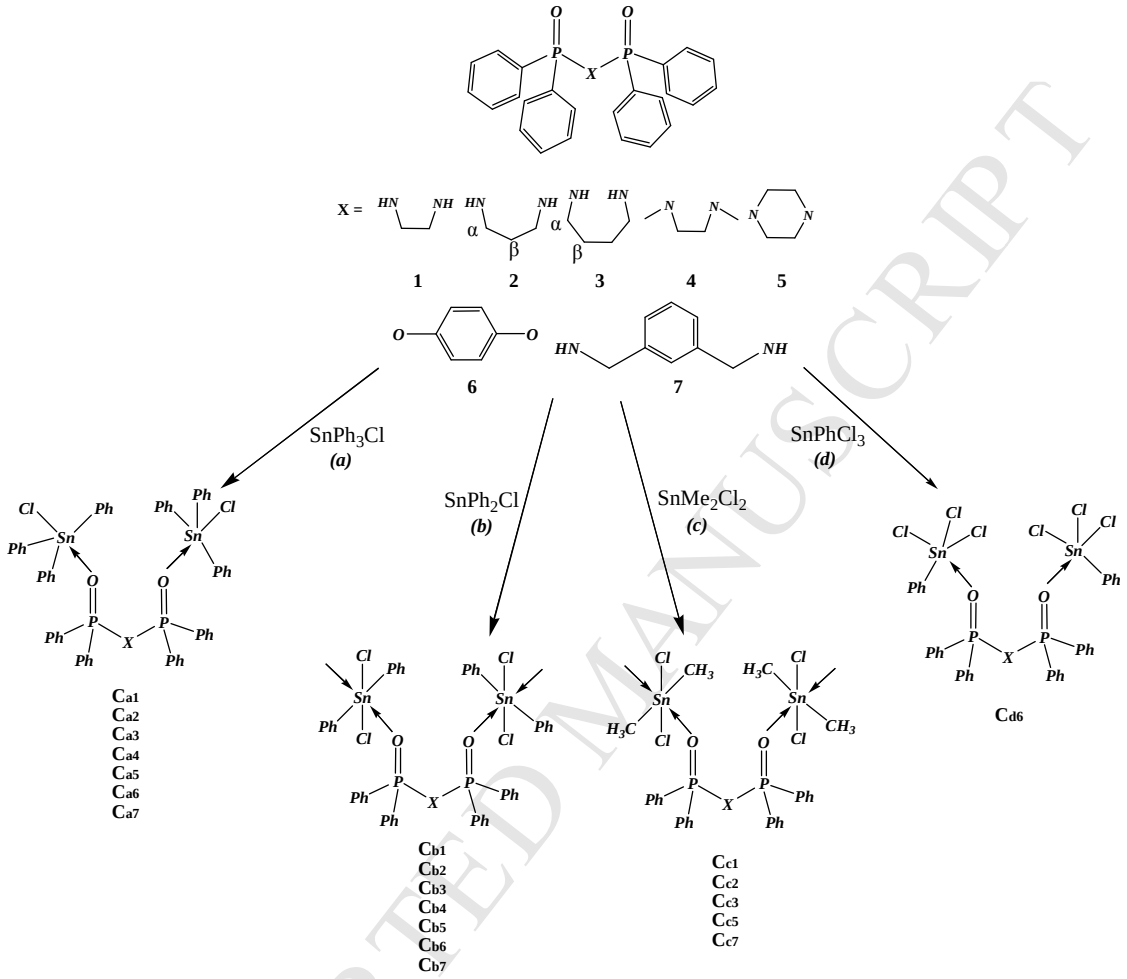

Scheme 1.

Highlights

- Organotin complexes of bisphosphoramidates were synthesized and characterized. QSAR models revealed that the descriptor of the electrophilicity (ω) parameter is correlated with the inhibition activity on *B. cereus*.
- X-Ray crystallography confirms the bridging ligands produce binuclear structures with $SnPh_3Cl$ acceptors and offer 1D polymeric arrangement toward $SnMe_2Cl_2$.

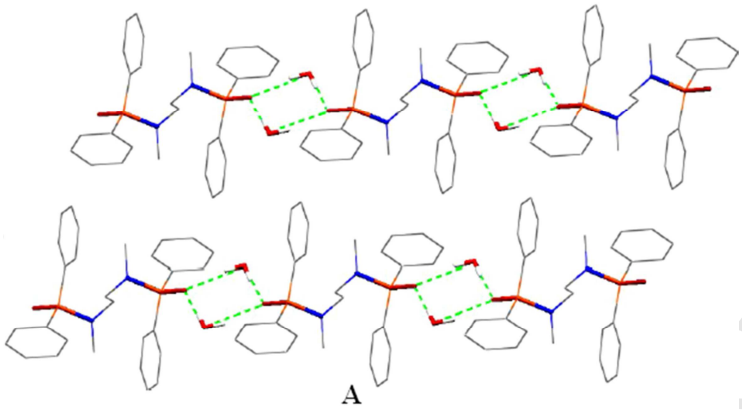

Fig. S1. Crystal packing of $\mathbf{L_4}$ along the *ac*-plane

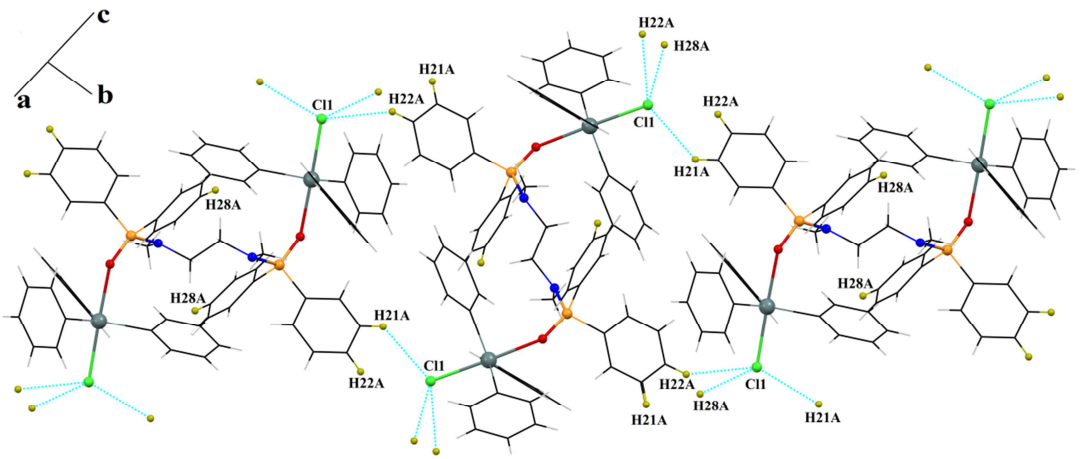

Fig. S2. Representation of CH…Cl interactions, resulting in 3D arrangements in $\mathbf{C_{a4}}$

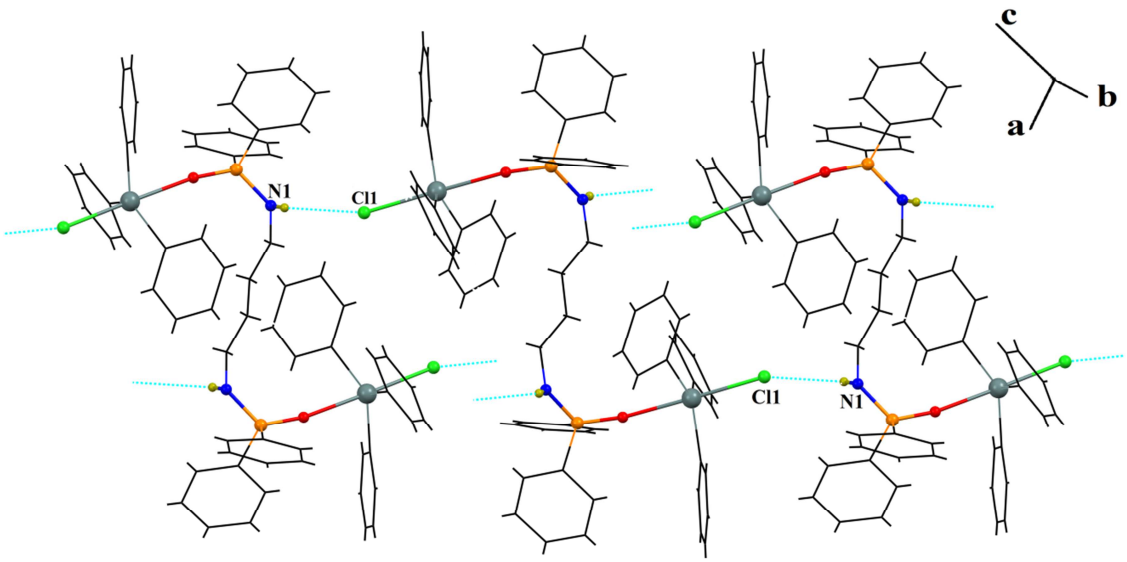

Fig. S3. Representation of NH…Cl and CH…Cl interactions, creating 2D aggregations in $\mathbf{C_{a3}}$

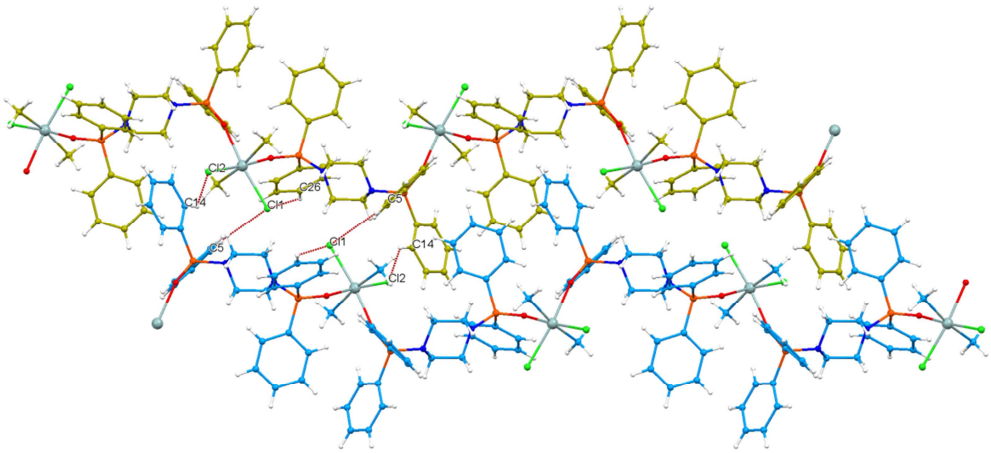

Fig. S4. Representation of CH…Cl interactions in $\mathbf{C_{c5}}$ (along the *bc*-plane), effective in the crystal packing